First-principles study of helium, carbon, and nitrogen in austenite, dilute austenitic iron alloys, and nickel

D. J. Hepburn,* D. Ferguson, S. Gardner, and G. J. Ackland†

Institute for Condensed Matter and Complex Systems, School of Physics and SUPA, The University of Edinburgh, Mayfield Road, Edinburgh EH9 3JZ, United Kingdom

(Received 22 January 2013; published 22 July 2013)

An extensive set of first-principles density functional theory calculations have been performed to study the behavior of He, C, and N solutes in austenite, dilute Fe-Cr-Ni austenitic alloys, and Ni in order to investigate their influence on the microstructural evolution of austenitic steel alloys under irradiation. The results show that austenite behaves much like other face-centered cubic metals and like Ni in particular. Strong similarities were also observed between austenite and ferrite. We find that interstitial He is most stable in the tetrahedral site and migrates with a low barrier energy of between 0.1 and 0.2 eV. It binds strongly into clusters as well as overcoordinated lattice defects and forms highly stable He-vacancy (V_mHe_n) clusters. Interstitial He clusters of sufficient size were shown to be unstable to self-interstitial emission and VHe_n cluster formation. The binding of additional He and V to existing V_mHe_n clusters increases with cluster size, leading to unbounded growth and He bubble formation. Clusters with n/m around 1.3 were found to be most stable with a dissociation energy of 2.8 eV for He and V release. Substitutional He migrates via the dissociative mechanism in a thermal vacancy population but can migrate via the vacancy mechanism in irradiated environments as a stable V_2He complex. Both C and N are most stable octahedrally and exhibit migration energies in the range from 1.3 to 1.6 eV. Interactions between pairs of these solutes are either repulsive or negligible. A vacancy can stably bind up to two C or N atoms with binding energies per solute atom up to 0.4 eV for C and up to 0.6 eV for N. Calculations in Ni, however, show that this may not result in vacancy trapping as VC and VN complexes can migrate cooperatively with barrier energies comparable to the isolated vacancy. This should also lead to enhanced C and N mobility in irradiated materials and may result in solute segregation to defect sinks. Binding to larger vacancy clusters is most stable near their surface and increases with cluster size. A binding energy of 0.1 eV was observed for both C and N to a [001] self-interstitial dumbbell and is likely to increase with cluster size. On this basis, we would expect that, once mobile, Cottrell atmospheres of C and N will develop around dislocations and grain boundaries in austenitic steel alloys.

DOI: 10.1103/PhysRevB.88.024115 PACS number(s): 61.72.−y, 61.82.Bg, 71.15.Mb, 75.50.Bb

I. INTRODUCTION

Steel, in its many forms, is the primary structural material in current fission and fusion systems and will be so for the foreseeable future. Carbon (C) and nitrogen (N) are both commonly found in steel, either as important minor alloying elements or as low-concentration impurities. In body-centered cubic (bcc) α-iron (α-Fe), it has been shown experimentally that C interacts strongly with vacancy point defects and more weakly with self-interstitial defects[1,2] and can form so-called Cottrell atmospheres around dislocations,[3] influencing yield properties and leading to strain aging of the material. First-principles (*ab initio*) calculations, as summarized in a recent review by Becquart and Domain,[4] support these findings and demonstrate that N exhibits similarly strong interactions. As such, both of these elements have a significant influence on microstructural evolution in bcc Fe, even down to very low concentrations, and a detailed understanding of their interactions and dynamics in steels is worthy of development, more generally.

Helium (He) is produced in significant quantities in the high neutron-irradiation fluxes typically experienced by the internal components of fission reactors and in the structural materials for fusion systems by (n,α) transmutation reactions. In combination with the primary point defect damage typical of irradiated environments, the presence of He plays a critical role in the microstructural evolution of these materials. As a result of its low solubility in metals, He becomes trapped in regions of excess volume, such as dislocations, grain boundaries, and, most strongly, vacancies and vacancy clusters.[5–12] As such, it aids the nucleation, stabilization, and growth of voids (He bubbles), resulting in swelling of the material.[10,13–16] The formation of He bubbles has also been implicated in high-temperature embrittlement of materials.[10,17,18] It is therefore of critical importance to gain a deep understanding of the behavior of He in these materials and the part it plays in the underlying mechanisms of microstructural evolution.

First-principles electronic structure calculations offer the most accurate means to develop an atomic level understanding of the dynamics and interactions of solutes and point defects in solids. As such, they play a central role in the development of a theoretical understanding of the microstructural evolution of irradiated materials, as part of a multiscale modeling approach, such as that used in the FP6 project, PERFECT,[19] and the FP7 project, PERFORM60.[20]

The behavior and interactions of He in a number of bcc and face-centered cubic (fcc) metals have been studied using density functional theory (DFT) techniques.[4,19,21–30] This database of He kinetics and interactions is essential for the interpretation of complex experimental results, such as those present in thermal He desorption spectra. A case in point is the work of Ortiz *et al.*,[31] who have developed a rate theory model based on DFT calculations of the kinetics and

interactions of point defects, He and C in bcc Fe (Refs. 25,31, and 33) The model successfully reproduces and interprets the existing experimental desorption results.[8] It is interesting to note that agreement with experiment was only possible once the effects of C were included, even though only 150 at. ppm of C was necessary; this again indicates the sensitivity of the microstructural evolution to C concentration. To date, however, there have been no *ab initio* studies of He in austenite, that is fcc γ-Fe, or austenitic FeCrNi alloys. This, primarily, is a result of the difficulty in describing the paramagnetic state of these materials.

Ab initio calculations have also been used to extensively study C (Refs. 4,31,32, and 34–38) and N (Refs. 4 and 35) in bcc Fe. These calculations show excellent agreement with experimentally verifiable parameters, such as the migration energy barrier for C diffusion, where *ab initio* values of 0.86 eV (Refs. 34 and 37), 0.87 eV (Ref. 38), and 0.90 eV (Ref. 35) are in good agreement with the experimental value of 0.87 eV (Refs. 2 and 39). For N, an equally good agreement is seen for the migration barrier, where a value of 0.76 eV was found by *ab initio* calculations[35] and a value of 0.78 eV was found experimentally.[40] Calculations in austenite are, however, limited primarily to solute dissolution, diffusion, and their influence on the electronic structure, local environment, and stacking fault energies,[34,41–46] although calculations of vacancy-C binding have been performed.[47]

In this work we present a detailed study of the energetics, kinetics, and interactions of He, C, and N solutes in model austenite and austenitic systems using DFT. A full treatment of paramagnetic austenite and FeCrNi austenitic alloys would naturally take into account the magnetic and composition dependence of the variables under study, and while *ab initio* techniques are now becoming available to model the paramagnetic state[48–51] and calculations in concentrated alloys are certainly achievable,[52] their complexity precludes a broad study of all the necessary variables relevant for radiation damage modeling. Previous studies have, instead, either taken ferromagnetic (fm) fcc nickel (Ni) as a model austenitic system[19,22,53] or modeled austenite using a small set of stable, magnetically ordered states, as in our previous work.[54] The advantage is that a more detailed study is possible, but the level of approximation involved is certainly not ideal and careful use should be made of the results obtained. Here, we follow the same approach used in our previous work,[54] performing our calculations in the two most stable ordered magnetic states of fcc Fe. In addition, we present and compare the results of corresponding calculations in fm Ni in order to make more general conclusions in Fe-Ni-based austenitic alloys.

In Sec. II we present the details of our calculations. We then proceed to present and discuss our results for He, C, and N solutes in defect-free austenite and dilute Fe-Cr-Ni austenitic alloys in Sec. III and their interactions with point defects and small vacancy clusters in Sec. IV before making our conclusions.

II. COMPUTATIONAL DETAILS

The calculations presented in this paper have been performed using the plane-wave DFT code, VASP,[55,56] in the generalized gradient approximation with exchange and correlation described by the parametrization of Perdew and Wang[57] and spin interpolation of the correlation potential provided by the improved Vosko-Wilk-Nusair scheme.[58] Standard projector augmented wave potentials[59,60] supplied with VASP were used for Fe, He, C, N, Ni, and Cr with 8, 2, 4, 5, 10, and 6 valence electrons, respectively. First-order ($N = 1$) Methfessel and Paxton smearing[61] of the Fermi surface was used throughout with the smearing width, σ, set to 0.2 eV to ensure that the error in the extrapolated energy of the system was less than 1 meV per atom. A 2^3 k-point Monkhorst-Pack grid was used to sample the Brillouin zone and a plane-wave cutoff of 450 eV. These pseudopotentials or exchange-correlation schemes are identical to a wide body of previous work, where they were chosen to ensure reasonable magnetic moments and atomic volumes.

All calculations used supercells of 256 ($\pm1, \pm2, \ldots$) atoms, with supercell dimensions held fixed at their equilibrium values and ionic positions free to relax. For the relaxation of single configurations, structures were deemed relaxed once the forces on all atoms had fallen below 0.01 eV/Å. For the nudged elastic band[62] (NEB) calculations used to determine migration barriers an energy tolerance of 1 meV or better was used to control convergence. Spin-polarized calculations have been performed throughout this work with local magnetic moments on atoms initialized to impose the magnetic state ordering but free to relax during the calculation. The relaxed local magnetic moments were determined by integrating the spin density within spheres centered on the atoms. Sphere radii of 1.302, 0.635, 0.863, 0.741, 1.286, and 1.323 Å were used for Fe, He, C, N, Ni, and Cr, respectively.

We have performed our calculations in both the face-centered tetragonal (fct) antiferromagnetic single layer (afmI) and double layer (afmD) collinear magnetic reference states for austenitic Fe (at $T = 0$ K), which we refer to as afmD Fe and afmI Fe, respectively, in what follows, using the same methodology as our previous work.[54] Both of these structures consist of (ferro-)magnetic (001) fcc planes, which we refer to as magnetic planes in what follows, but with opposite magnetic moments on adjacent planes in the afmI state and an up,up,down,down ordering of moments in adjacent magnetic planes in the afmD state. The fcc fm and fct fm states were found to be structurally unstable and spontaneously transformed upon addition of a whole range of defects and solutes.[54] The fcc ferromagnetic high-spin (fm-HS) state was, however, found to be stable to isotropic effects and we have performed a select few calculations in this state for comparison with other work in the literature.[34] We have previously attempted to use randomly disordered moments to represent paramagnetism[49,51,54] and found that but for migration processes (and some relaxations) the spins spontaneously reorient, making it impossible to define a reference state. This is probably due to the low-symmetry configurations required and the low paramagnetic transition temperature in Fe. We have also performed a number of calculations in fcc fm Ni, which we refer to, simply, as Ni in what follows, where these results were not available in the literature. We take the lattice parameters for afmI Fe as $a = 3.423$ Å and $c = 3.658$ Å, those for afmD Fe as $a = 3.447$ Å and $c = 3.750$ Å and take $a = 3.631$ Å for fm-HS Fe. Calculations in Ni have been performed with an equilibrium lattice parameter of $a = 3.522$ Å. The

corresponding magnitudes for the local magnetic moments in bulk, equilibrium afmI, afmD, and fm-HS Fe were determined as 1.50, 1.99, and 2.57 μ_B, respectively,[54] and a local moment of 0.59 μ_B was found in bulk, equilibrium Ni. Convergence tests indicated that local moments were determined to a few hundredths of μ_B.

We use elastic constants for our reference states, as determined previously,[54] or determined here using the same techniques. For fm-HS Fe, we find $C_{11} = 40$ GPa, $C_{12} = 240$ GPa, and $C_{44} = -10$ GPa, which clearly shows instability to shear strains and tetragonal deformations, as $C' = C_{11} - C_{12} = -200$ GPa. It is, however, stable to isotropic deformations as the bulk modulus, $B = 187$ GPa, is positive. For Ni, we find $C_{11} = 272$ GPa, $C_{12} = 158$ GPa, and $C_{44} = 124$ GPa, which gives $C' = 114$ GPa and $B = 196$ GPa, and shows that this material is stable to any strain deformations.

We have determined the solution enthalpy for carbon in Fe and Ni using diamond as a reference state. The diamond structure was determined using the same settings as our other calculations but with sufficient k-point sampling to ensure absolute convergence of the energy. We found a lattice parameter of $a = 3.573$ Å, in good agreement with the standard experimental value.

We define the formation energy, E_f, of a configuration containing n_X atoms of each element, X, relative to a set of reference states for each element using

$$E_f = E - \sum_X n_X E_X^{\text{ref}}, \tag{1}$$

where E is the calculated energy of the configuration and E_X^{ref} is the reference state energy for element, X. We take the reference energies for Fe, Ni, and Cr to be the energies per atom in the bulk metal, that is, Fe in either the afmI, afmD, or fm-HS states, as appropriate, Ni in its fcc fm ground state, and Cr in its bcc antiferromagnetic (afm) ground state. Details of the Fe and Ni reference states are given above, whereas for Cr an equilibrium lattice parameter of 2.848 Å was found with a corresponding local moment of magnitude 0.87 μ_B. For He, C, and N the reference states were taken to be the nonmagnetic free atom, as calculated in VASP.

In a similar manner, we define the formation volume at zero pressure, V_f, of a configuration relative to the bulk metal by

$$V_f = V(0) - n_{\text{bulk}} V_{\text{bulk}}, \tag{2}$$

where $V(0)$ is the volume of the configuration at zero pressure, n_{bulk} is the number of bulk (solvent) metal atoms in the configuration and V_{bulk} is the volume per atom in the defect-free bulk metal, which we found to be 11.138, 10.712, 11.970, and 10.918 Å^3 in afmD Fe, afmI Fe, fm-HS Fe, and Ni, respectively. For our calculations, $V(0)$ was determined by extrapolation from our calculations at the fixed equilibrium volume using the residual pressure on the supercell and the bulk modulus for the defect-free metal.

We define the binding energy between a set of n species, $\{A_i\}$, where a species can be a defect, solute, clusters of defects and solutes, etc., as

$$E_b(A_1, \ldots, A_n) = \sum_{i=1}^{n} E_f(A_i) - E_f(A_1, \ldots, A_n), \tag{3}$$

where $E_f(A_i)$ is the formation energy of a configuration containing the single species, A_i, and $E_f(A_1, \ldots, A_n)$ is the formation energy of a configuration containing all of the species. With this definition an attractive interaction will correspond to a positive binding energy. One intuitive consequence of this definition is that the binding energy of a species, B, to an already existing cluster (or complex) of species, $\{A_1, \ldots, A_n\}$, which we collectively call C, is given by the simple formula

$$E_b(B,C) = E_b(B, A_1, \ldots, A_n) - E_b(A_1, \ldots, A_n). \tag{4}$$

This result will be particularly useful when we consider the additional binding of a vacancy or solute to an already existing vacancy-solute complex.

We have quantified a number of uncertainties in the formation and binding energies presented in this work. Test calculations were performed to determine the combined convergence error from our choice of k-point sampling and plane-wave cutoff energy. For interstitial C and N solutes in a defect-free lattice, formation energies were converged to less than 0.05 eV and formation energy differences, such as migration energies, to less than 0.03 eV. For interstitial He the convergence errors were half of those for C and N. For configurations containing vacancies or self-interstitial defects, formation energies were converged to 0.03 or 0.07 eV, respectively, while binding energies were converged to 0.01 eV, except for the binding of He to a vacancy, where the error was 0.03 eV.

The zero-point energy (ZPE) contributions to the formation energy, which can be significant for light solute atoms, have not been calculated in this work. We performed calculations of the ZPE for He, C, and N solutes in a number of test sites in afmD and afmI Fe, keeping the much heavier Fe atoms fixed, which is equivalent to assuming they have infinite mass.[34] The results showed that the ZPE contributions were consistently around 0.10 eV in all cases, which we take as an estimate of the ZPE error on the formation energies of configurations containing C, N, and He. The variation with site was, however, surprisingly low at 0.01 eV, which we take as an estimate of the ZPE error in formation energy differences, binding energies, and the solution enthalpy for C, given that ZPE contribution in graphite is very similar to in Fe (Ref. 34).

Performing calculations in a fixed supercell of volume, V, results in a residual pressure, P, for which an Eshelby-type elastic correction to the total and, therefore, formation energy[63,64] of $E^{\text{corr.}} = -P^2V/2B$, can be applied. As such, $E^{\text{corr.}}$ also serves to indicate the likely finite-volume error. For many of the configurations considered here these corrections are negligible compared to other sources of error. Where they are significant, however, their relevance is discussed at the appropriate points in the text.

III. SOLUTES IN THE DEFECT-FREE LATTICE

A. Single solutes

The formation energies for substitutionally and interstitially sited He, C, and N solutes in the sites shown in Fig. 1 are given in Table I for Fe and Table II for Ni. We found that the Eshelby corrections were negligible for substitutional He but could be as high as 0.02 eV in magnitude for interstitial He and 0.04 eV

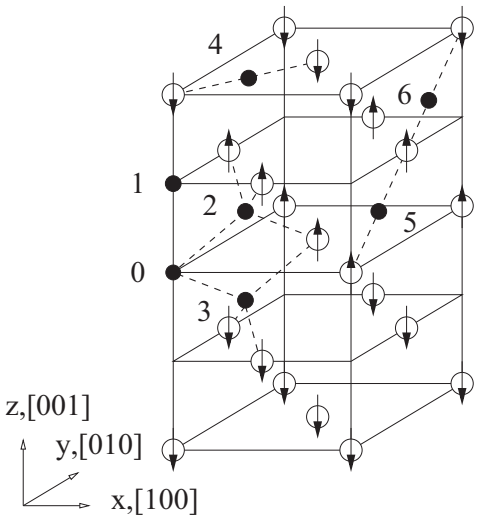

FIG. 1. Substitutional (0) and interstitial octahedral (1), tetrahedral (2-3), and crowdion (4-6) positions (in black) in afmD Fe. The Fe atoms are shown in white with arrows to indicate the local moments. Magnetic planes are included to aid visualization. The afmD Fe state, which has the lowest symmetry, is shown to uniquely identify all distinct positions. In afmI Fe and Ni, positions 2 and 3 are equivalent by symmetry, as are 5 and 6. In Ni, position 4 is also equivalent to 5 and 6.

for interstitial C and N. The corresponding uncertainties in formation energy differences were around half of these values. We discuss the results for He first, followed by those for C and N.

1. He solute

We found that He exhibits a large, positive formation energy in all sites but is most stable substitutionally, which is consistent with existing DFT studies of He in other bcc and fcc metals.[4,19,21–30] The standard explanation is that, as a closed-shell noble-gas element, bonding interactions should be primarily repulsive, leading to insolubility and a preference for sites with the largest free volume.[21,26] This result distinguishes He from other small solutes, such as C and N, which are more stable interstitially but also distinguishes it from substitutional alloying elements, such as Ni and Cr with formation energy differences between substitutional and interstitial sites in Fe of 3.0 eV and above.[54,65]

In Fe, the influence of substitutional He on the local magnetic moments of atoms in its first-nearest-neighbor (1nn) shell was found to be similar to those for a vacancy, being generally enhanced relative to the bulk moment and by up to 0.38 μ_B here. This is similar to He in bcc Fe (Refs. 25 and 26). Indeed, we found that if the He atom was removed from the relaxed substitutional configuration with no further relaxation, the local 1nn Fe moments changed by less than

TABLE II. Formation energies, E_f, in eV, for substitutionally and interstitially sited He, C and N atoms in Ni. The layout and data content is as in Table I.

Config.	He E_f (ΔE_f)	C E_f (ΔE_f)	N E_f (ΔE_f)
sub (0)	**3.185**	−5.386	−4.562
	(—)	(—)	(—)
octa (1)	4.589	**−8.422**	**−7.520**
	(0.129)	(0.000)	(0.000)
tetra (2-3)	**4.460**	−6.764	−6.497
	(0.000)	(1.659)	(1.023)
⟨110⟩ crow. (4-6)	4.651	−6.795	−5.970
	(0.191)	(1.628)	(1.550)

TABLE I. Formation energies, E_f, in eV, for substitutionally and interstitially sited He, C and N atoms in austenite, as shown in Fig. 1. The formation energies in bold are for the most stable states. For He, which is most stable substitutionally, the most stable interstitial site is also highlighted. The formation energy differences, ΔE_f (in brackets), to the most stable interstitial configurations are also given, in eV. Where the configuration was found to be unstable the configuration to which it relaxed is given. The substitutional N configuration in the fct afmD state relaxed to one with an octa N at 1 nn to a vacancy.

	He		C		N	
Config.	afmD Fe E_f (ΔE_f)	afmI Fe E_f (ΔE_f)	afmD Fe E_f (ΔE_f)	afmI Fe E_f (ΔE_f)	afmD Fe E_f (ΔE_f)	afmI Fe E_f (ΔE_f)
sub (0)	**4.024**	**4.185**	−6.981	−6.244	rlx (other)	−5.153
	(—)	(—)	(—)	(—)		(—)
octa (1)	4.669	5.026	**−8.797**	**−8.856**	**−8.602**	**−8.621**
	(0.206)	(0.059)	(0.000)	(0.000)	(0.000)	(0.000)
tetra uu (2)	4.529	as	−6.535	as	−6.917	as
	(0.066)	tetra ud	(2.261)	tetra ud	(1.685)	tetra ud
tetra ud (3)	**4.464**	**4.967**	−6.644	−6.272	−7.044	−6.737
	(0.000)	(0.000)	(2.153)	(2.585)	(1.558)	(1.884)
[110] crow. (4)	rlx (3)	5.271	−6.764	−6.412	rlx (3)	−6.006
		(0.303)	(2.033)	(2.445)		(2.614)
[011] crow. uu (5)	4.827	as	−7.354	as	−7.000	as
	(0.364)	[011] crow. ud	(1.443)	[011] crow. ud	(1.602)	[011] crow. ud
[011] crow. ud (6)	4.802	5.188	−7.487	−6.744	−7.218	−6.328
	(0.338)	(0.221)	(1.310)	(2.113)	(1.384)	(2.293)

0.03 μ_B. In contrast to the vacancy, however, where 1nn Fe were displaced inwards by 0.09 and 0.02 Å in afmD and afmI Fe, respectively,[54] the respective displacements around a substitutional He were, on average, outwards by 0.02 and 0.04 Å. This contrast can also be seen in the formation volumes, which were found to be $0.74V_{bulk}$ and $0.96V_{bulk}$ for a vacancy, compared to $1.17V_{bulk}$ and $1.38V_{bulk}$ for substitutional He in afmD and afmI Fe, respectively. Results in Ni were very similar to Fe, with enhanced moments in the 1nn shell around both a vacancy and substitutional He, a contraction of 0.04 Å in the 1nn shell around a vacancy, and an expansion of 0.02 Å around substitutional He. The formation volume for substitutional He, at $1.02V_{bulk}$, was again found to be greater than that for the vacancy, at $0.66V_{bulk}$.

The large formation energy difference, of around 2 eV, between substitutional He and the underlying vacancy in Fe and Ni (see Sec. IV), which must be due to chemical interactions, may seem at odds with the relatively inert behavior of He mentioned above. However, similar results in bcc Fe have been reproduced using simple pair potentials,[66,67] which demonstrates that such a large energy difference, once distributed over 1nn and 2nn bonds, is commensurate with the relatively small forces observed on the neighboring Fe atoms around substitutional He.

In Fe, interstitial He was found to be most stable in the tetrahedral (tetra) site, the octahedral (octa) site being the next most stable and lying 0.206 and 0.059 eV higher in energy in the afmD and afmI states, respectively. There is no consistent ordering of the octa and tetra sites in *ab initio* studies of other fcc metals, with the octa site being most stable in Ag (Ref. 21), Al (Ref. 23), and Pd (Ref. 24 and 24) and the tetra site being most stable in Cu (Ref. 21) and Ni (Refs. 19,21, and 22), as our results for Ni confirm. In both Fe and Ni, however, He favors the tetra site, which gives a strong indication that the tetra site will also be the most stable interstitial site in concentrated Fe-Ni-based austenitic alloys.

The other interstitial sites considered here lie no more than 0.364 eV above the tetra site, suggesting many low-energy migration paths for interstitial He, that is, in the absence of any lattice defects that can act as strong traps. The bilayer structure in afmD Fe breaks the symmetry of the octa site and a He atom placed there was found to spontaneously relax in the $[00\bar{1}]$ direction (as defined in Fig. 1), to between layers of the same spin by 0.55 Å. It is, perhaps, surprising that in both afmI Fe and Ni, an octa-sited He was also found to be unstable to small displacements in many directions. We present the results of these calculations in Table III.

It is particularly clear in the afmI Fe data that lower energy configurations were found along all of our test directions, with He relaxing to between 0.23 and 0.62 Å from the symmetrical position. The picture is less clear in afmD Fe, where He was generally found to relax to the lowest local energy minimum but other metastable positions were found. In Ni, the drop in energy is far less pronounced than in Fe but is still present, with He relaxing to stable positions 0.29 Å from the center along ⟨100⟩ directions and 0.54 Å along ⟨110⟩ directions. These configurations are important, certainly as intermediate states for the migration of interstitial He, but also as potential transition states and already suggest a low migration-energy barrier. We study these possibilities in detail in Sec. III B.

TABLE III. Formation energies, E_f, and formation energy differences, ΔE_f, in eV, to the most stable tetra site (in brackets) for octa-sited He atoms in Fe. He is either sited symmetrically (sym.) or has been displaced off center, in which case the direction of the displacement is used to label the configuration and the displacement length after relaxation, Δr, is given, in Å. The symmetrical position is as shown in Fig. 1 and directions determined from that point with the coordinate system shown. When no stable local energy minimum was found the state to which the configuration relaxed is given.

	afmD Fe		afmI Fe		Ni	
Config.	E_f (ΔE_f)	Δr	E_f (ΔE_f)	Δr	E_f (ΔE_f)	Δr
octa sym.	rlx octa $[00\bar{1}]$		5.208 (0.241)	0.00	4.617 (0.157)	0.00
octa [100]	rlx octa $[00\bar{1}]$		5.105 (0.138)	0.39	4.607 (0.147)	0.29
octa [001]	4.812 (0.348)	0.30	5.026 (0.059)	0.50	as octa [100]	
octa $[00\bar{1}]$	4.669 (0.206)	0.58	as octa [001]		as octa [100]	
octa [110]	rlx octa $[00\bar{1}]$		5.079 (0.112)	0.54	4.589 (0.129)	0.54
octa [011]	4.799 (0.335)	0.58	5.035 (0.068)	0.23	as octa [110]	
octa $[01\bar{1}]$	rlx octa $[00\bar{1}]$		as octa [011]		as octa [110]	
octa [111]	rlx tetra ud		5.029 (0.062)	0.62	rlx tetra	
octa $[11\bar{1}]$	rlx octa $[00\bar{1}]$		as octa [111]		as octa [111]	

For completeness, we also tested for the presence of stable off-center positions for tetra-sited He but relaxation always returned He to the symmetrical position.

The displacements of 1 nn Fe atoms around interstitially sited He were, unsurprisingly, found to be greater than for the substitutional site. A tetra-sited He in afmI Fe displaced its neighbors by 0.23 Å. In afmD Fe, displacements of 0.22 and 0.32 Å were found for tetra uu- and tetra ud-sited He, respectively. The magnetic moments on the 1 nn Fe atoms were quenched relative to the bulk moments by 0.24 μ_B in afmI Fe and by 0.16 μ_B for the tetra uu site in afmD Fe but enhanced by 0.15 μ_B for the tetra ud site. We attribute this difference to the greater free volume into which 1 nn Fe atoms around a tetra ud site may be displaced. We found formation volumes of $0.82V_{bulk}$ and $0.99V_{bulk}$ for tetra-sited He in afmI Fe and tetra-ud-sited He in afmD Fe, respectively. Once again, results in Ni were similar to Fe, with a 0.24 Å displacement and moment quench of 0.09 μ_B in 1 nn Ni atoms around a tetra-sited He and a formation volume of $0.78V_{bulk}$.

In the most stable octa configuration in Fe, the local geometry is complicated by the displacement of He from the symmetrical position. For that reason, we define a local unit cell surrounding the octa site using the positions of its six 1 nn metal atoms, which lie at the centers of the cell faces, and report on the lattice parameters of that cell. In both

afmI and afmD Fe, the local lattice parameter along [100] and [010] directions, a_{1nn}, is increased by 0.31 Å relative to the bulk equilibrium lattice, with the local lattice parameter along the [001] direction, c_{1nn}, exhibiting an increase of 0.26 Å in the afmD state and 0.29 Å in the afmI state. The local moment on the 1nn Fe atom that He is displaced towards is significantly quenched by 1.04 and 0.41 μ_B in the afmD and afmI states, respectively. In contrast, the other 1 nn moments are moderately enhanced by between 0.03 and 0.17 μ_B. In Ni, the most stable off-center octa position is along ⟨110⟩ directions from the symmetrical position. The resulting local unit cell, which exhibits a very slight shear, has $c_{1nn} \neq a_{1nn}$, with a_{1nn} increased by 0.31 Å relative to bulk and c_{1nn} by 0.28 Å. Local 1 nn Ni moments were found to be quenched by between 0.02 and 0.08 μ_B.

These findings suggest that the relative stability of tetra over octa He, which is opposite to the order suggested by free volume arguments,[21,26] may be best ascribed to the relative ease with which a tetra He may lower its purely repulsive interactions with neighboring atoms by local dilatation. To further investigate this hypothesis in Fe we split the formation energy for unrelaxed and relaxed substitutional octa and tetra He configurations into three terms, in a similar manner to that in the work of Fu *et al.*[38] The first is the formation energy, $E_f^{def.}$, of any underlying, atomically relaxed, defects, e.g., a single vacancy for substitutional He. The second is the mechanical energy, $E_f^{mech.}$, required to deform the Fe matrix containing those relaxed defects to the exact positions found in the configuration under study. The third is the energy change from chemical interactions, $E_f^{chem.}$, upon insertion of the solute into its final position with no further relaxation. We also define the insertion energy, $E_f^{ins.}$, as the sum of $E_f^{mech.}$ and $E_f^{chem.}$, i.e., the formation energy for insertion of a solute into any position in a relaxed Fe matrix containing any relevant defects. We take the insertion energy as a more appropriate measure of site preference than the (total) formation energy, E_f. The results are given in Table IV.

TABLE IV. Mechanical deformation energy, $E_f^{mech.}$, and chemical bonding energy, $E_f^{chem.}$, contributions to the total formation energy, E_f, and the insertion energy, $E_f^{ins.}$, for unrelaxed and relaxed substitutional, tetra and octa He solute configurations in afmD and afmI Fe, in eV. The most stable octa configuration was used in both states and the tetra ud configuration was used for the afmD state.

Config.	$E_f^{mech.}$	$E_f^{chem.}$	$E_f^{ins.}$
	afmD Fe + He		
sub, unrelaxed	0.136	2.150	2.286
sub, relaxed	0.167	2.045	2.212
tetra, unrelaxed	0.000	6.778	6.778
tetra, relaxed	1.330	3.134	4.464
octa, unrelaxed	0.000	5.804	5.804
octa, relaxed	0.755	3.914	4.669
	afmI Fe + He		
sub, unrelaxed	0.023	2.662	2.685
sub, relaxed	0.155	2.073	2.228
tetra, unrelaxed	0.000	6.774	6.774
tetra, relaxed	0.999	3.968	4.967
octa, unrelaxed	0.000	6.081	6.081
octa, relaxed	0.855	4.171	5.026

The substitutional site is clearly the most favored, even in the unrelaxed state and by at least 2.25 eV once relaxed. In the unrelaxed lattice, an octa He is significantly more stable than a tetra He, as expected from purely repulsive interactions given the relative proximity of 1 nn Fe in the two sites. Under relaxation the chemical bonding energy is significantly reduced and to a far greater degree in the tetra site. The positive mechanical deformation energy is also greater for tetra He but the net result is still to stabilize tetra over octa He. These results clearly show that the relative stability of He in tetra and octa sites can be understood as resulting from a balance between the energy required for local dilatation of the Fe matrix coupled with a purely repulsive Fe-He interaction, which we suggest could be easily modeled using a simple pair potential.

In bcc Fe, the relative stability of tetra over octa He has been explained as resulting from strong hybridization of He *p* states with Fe *d* states.[21,26] However, we do not find the evidence for such strong hybridization to be convincing. We suggest that a repulsive nonbonding mechanism also applies to bcc Fe and explains the difference in a much simpler manner. The magnetic and polarization effects discussed by Seletskaia *et al.*[26] and Zu *et al.*[21] are a simple consequence of these nonbonding interactions and not He *p*-state, Fe *d*-state hybridization. Formation energy calculations[21,26] show that octa-sited He is higher in energy both before and after relaxation, despite the relaxation energy for octa He being greater than for tetra He. This results, primarily, from the very short 1 nn Fe-He separations in the octa site when compared to those for the tetra site and the relative strengths of the resulting repulsive interactions. The fact that purely repulsive pair potentials for Fe-He interactions in bcc Fe are capable of reproducing the relative stability[66,67] gives further support to our claim.

2. *C and N solutes*

The results for C and N solutes (in Tables I and II) show that both elements clearly favor the octa interstitial site in both Fe and Ni. Experimental observations show this to be the preferred site for C in an Fe-13wt%Ni-1wt%C austenitic alloy.[68] One exception worth comment is that of substitutional C in afmD Fe, for which the insertion energy, $E_f^{ins.}$, which as discussed for He provides a more appropriate measure of site preference, is comparable to that for octa C. On further inspection we found that, due to the asymmetries in the afmD state, the initially on-lattice C atom relaxed to 0.77 Å from the lattice site. While this displacement is certainly significant, the C atom remains closer to the substitutional site than to an octa position at 1 nn to the (vacated) lattice site and has been named to reflect this difference. Relaxation of the substitutional N configuration also resulted in displacement away from the lattice site but convergence was to a configuration with the N atom in an octa site at 1 nn to a vacancy. We performed calculations to test for the presence of any stable off-center octa configurations for C and N but none were found, in contrast to the results for He.

We discuss the influence of octa C and N solutes on the local lattice geometry in an identical manner to octa-sited He, that is, using a_{1nn} and c_{1nn}. The results are presented in Table V for both Fe and Ni, including results in fm-HS Fe, which was shown to be mechanically unstable in our previous

TABLE V. Lattice parameter differences (Δa_{1nn} and Δc_{1nn}, in Å) between those for the unit cell surrounding octa C and N solutes (a_{1nn} and c_{1nn}) and the bulk equilibrium lattice parameters and the local c_{1nn}/a_{1nn} ratio. Linear expansion coefficients ($\Delta a/(ax_X^f)$ and $\Delta c/(cx_X^f)$) for the dependence of the lattice parameters on the fractional atomic solute composition, x_X^f, for solute X. For afmD and afmI Fe, the linear expansion coefficient for an effective lattice parameter, defined by $a_{eff.} = (a^2c)^{1/3}$ is also given. Fractional formation volumes, V_f/V_{bulk} for octa-sited C and N solutes are given. The solution energy, $E_{f,G}^{sol.}$, taken to dissolve graphite in each of the reference states is given, in eV. For comparison, our calculations in bcc fm Fe give $E_{f,G}^{sol.} = 0.700$ eV.

	afmD Fe		afmI Fe		fm-HS Fe		Ni	
	C	N	C	N	C	N	C	N
Δa_{1nn}	0.321	0.303	0.305	0.276	0.174	0.145	0.183	0.170
Δc_{1nn}	0.080	0.048	0.154	0.127				
c_{1nn}/a_{1nn}	1.016	1.013	1.023	1.023				
$\Delta a/(ax_X^f)$	0.266	0.265	0.341	0.327	0.072	0.034	0.243	0.263
$\Delta c/(cx_X^f)$	−0.057	−0.044	0.026	0.042				
$\Delta a_{eff.}/(a_{eff.}x_X^f)$	0.158	0.162	0.236	0.232				
V_f/V_{bulk}	0.53	0.54	0.78	0.76	0.214	0.102	0.73	0.79
$E_{f,G}^{sol.}$	0.323		0.263		−0.164		0.697	

work,[54] but not to the isotropic strain exerted locally by an octa-sited solute. We include this extra state here to compare with the work of Jiang and Carter.[34] It is immediately clear that the geometrical influence of octa C is rather similar to octa N, although with slightly smaller dilatations for N. Local expansion is observed in all our reference states, although the expansion of c in afmD and afmI Fe is much less than for a. As a result, the local c/a ratio is significantly reduced relative to the bulk material, to 1.02 around a C solute in both afmD and afmI Fe, which is in good agreement with the 3% tetragonal distortion found by Boukhvalov *et al.*,[42] and to 1.01 and 1.02 around an N solute in afmD and afmI Fe, respectively.

The magnetic influence of octa C and N solutes is, again, very similar with significant quenching of the local moments on 1 nn solvent atoms seen in all reference states, as expected for magnetic atoms under compression. In both afmD and afmI Fe the effect is most pronounced in those neighbors lying within the same magnetic plane as the solute, which also show the most significant displacement, resulting in a quench of 0.72(0.66) μ_B for C(N) in afmD Fe and of 1.25(1.37) μ_B in afmI Fe. In fm-HS Fe, 1 nn moments are quenched by 0.48(0.57) μ_B around C(N) and in Ni a quench of 0.42 μ_B was observed for both C and N.

In addition to this local influence, we have investigated the dependence of the lattice parameters of our reference states on the fractional atomic compositions, x_C^f and x_N^f for C and N, respectively. For low concentrations, as studied here, the lattice parameters change linearly as a function of the fractional composition.[69] In this case, quantities such as $\Delta a/(ax_C^f)$, where Δa is the difference between the lattice parameter with and without solute atoms present, are dimensionless constants that completely specify the linear expansion. Our calculations have been performed in supercells at the equilibrium lattice parameters, so we determine the linear expansion coefficients by extrapolating to zero stress using the residual stress that builds up on the supercell upon addition of a solute and a knowledge of the elastic constants (see Sec. II). In afmD and afmI Fe we have also calculated the linear expansion coefficients for an effective lattice parameter, $a_{eff.} = (a^2c)^{1/3}$, as a means to compare more directly with experiment.

The results (in Table V) show that local expansion around the solutes leads to a net expansion of the cell overall. The afmD state of Fe does, however, exhibit a small contraction in c and the afmI state shows very little expansion in c, when compared to that for a. Once again, this shows that the addition of C and N acts to reduce the c/a ratio, bringing the lattice back toward perfect fcc. In austenite, experimental results by Cheng *et al.*[69] and presented by Gavriljuk *et al.*[41] show that $\Delta a/(ax_C^f)$ lies between 0.199 and 0.210, with $\Delta a/(ax_N^f)$ being slightly greater at between 0.218 and 0.224. Our results in afmD and afmI Fe are in broad agreement with these values but do not differentiate between C and N. Results in fm-HS Fe are significantly different from experiment, which again shows the unsuitability of this state for modeling austenite. It is interesting to note that our results for Ni are consistent with those for austenite and do exhibit more expansion due to N than for C. Experimental results in austenitic FeCrNi alloys[41] are comparable to those for pure austenite and the general agreement with our results strengthens the case for using afmD and afmI Fe or using Ni as model systems for austenite and austenitic alloys.

We have determined the solution energy at fixed equilibrium volume, $E_{f,G}^{sol.}$, taken to dissolve graphite into our four bulk states (Table V). We have done this by calculating the solution energy relative to diamond and then applying the commonly accepted experimental energy difference of 20 meV/atom between the cohesive energies of diamond and graphite at $T = 0$ K (Ref. 70). For comparison, we have calculated $E_{f,G}^{sol.}$ for C in bcc fm Fe and find a value of 0.70 eV, which is in good agreement with the experimental value of between 0.60 and 0.78 eV found by Shumilov *et al.*[34,71]

The solution energies in all three Fe states are significantly lower than for bcc fm Fe. This is consistent with the relatively higher solubility of C in austenite than in ferrite and with the well-known experimental result that C stabilizes austenite over ferrite, as seen in the phase diagram. The effect is most pronounced in the fm-HS state, where the reaction is exothermic, in good agreement with previous DFT calculations.[34] In combination with the results discussed above, this implies that at sufficient concentrations, C will act to stabilize the

fm-HS state over the others, just as was found for Ni in fcc Fe-Ni alloys.[72] The same conclusions follow for N by a direct comparison of the formation energies for octa sited N (see Table I), for which we found values of −8.252 and −9.018 eV in bcc fm and fcc fm-HS Fe, respectively.

Experimental results for the solution enthalpy of C in austenite[73] yield a value of $E_{\mathrm{f,G}}^{\mathrm{sol.}} = 0.37$ eV at the concentration studied here, which agrees to within 0.1 eV with our calculations in afmD and afmI Fe but not with those for the fm-HS state and again supports their suitability as reference states for paramagnetic austenite. Our calculations in the ferromagnetic state for Ni are in good agreement with previous DFT calculations of Siegel and Hamilton.[74] However, as they report, this value is higher than those found experimentally in high-temperature, paramagnetic Ni, which lie between 0.42 and 0.49 eV. It is worth noting that their calculations in nonmagnetic (nm) Ni, which they use to model the paramagnetic state, underestimate the experimental range at between 0.2 and 0.35 eV. We conclude that the calculated solution enthalpy for C in Ni is particularly sensitive to the underlying magnetic state.

B. Solute migration

As a first step in the calculation of migration energies for He, C, and N solutes we investigated whether a 32-atom cell would be sufficient for this purpose. To do this we recalculated the formation energies for substitutional and interstitial He and C in afmD Fe using a 32-atom cell. We compare these with our 256-atom cell calculations (Table I) in Table VI.

There is a significant size effect on the formation energies in the 32-atom cell, except for substitutional He and octa C, where the formation energies are within errors of those in the 256-atom cell. The formation energies are greater in the 32-atom cell, as expected from volume-elastic effects, by between 0.06 and 0.12 eV for interstitial He and by between 0.00 and 0.37 eV for interstitial C. Formation energy differences to the most stable interstitial configuration also exhibit a significant size effect, with the smaller cell underestimating them by between 0.04 and 0.06 eV for He configurations and overestimating them by between 0.10 and 0.37 eV for C. It is reasonable to assume that the migration energy, which is itself a formation energy difference, will suffer from similar size effects.

For C, the choice of cell size actually changes the relative stability of the [110] crowdion and tetra ud configurations. This is important as these two are transition states on two distinct migration paths for C (as will be shown in what follows). The small cell would, therefore, give the wrong minimum energy path (MEP), as found previously for C in fm-HS Fe (Ref. 34). Closer inspection of the [110] crowdion configuration showed that the periodic boundary conditions in the smaller cell applied unphysical constraints on the displacements of Fe atoms at 1 nn to C and along the crowdion axis generally, which resulted in a significant buckling, moving the C atom towards the tetra uu site, that is along [001], by 0.71 Å. In the larger cell these constraints are not present, resulting in a significantly lower formation energy and while there is still a small displacement towards the tetra uu site of 0.18 Å this is to be expected given the asymmetry present in the afmD state.

TABLE VI. Comparison between calculations in 32-atom and 256-atom cells in afmD Fe of the formation energies, E_{f}, in eV, for substitutional and interstitial He and C solutes and formation energy differences, ΔE_{f}, in eV, to the most stable interstitial configurations, highlighted in bold. The layout and data content of each column is as in Table I. The column headed "32 atom" contains the results for the 32-atom cell and the column headed "Error" contains the difference between the 32-atom and 256-atom results, which we take as an estimate of the finite volume error in the 32-atom cell.

	He		C	
Config.	32 atom E_{f} (ΔE_{f})	Error E_{f} (ΔE_{f})	32 atom E_{f} (ΔE_{f})	Error E_{f} (ΔE_{f})
Sub (0)	**4.039** (—)	**0.015** (—)	−6.911 (—)	0.070 (—)
octa (1)	4.730 (0.151)	0.061 (−0.055)	**−8.798** (0.000)	−0.001 (0.000)
tetra uu (2)	4.607 (0.028)	0.078 (−0.038)	−6.395 (2.403)	0.140 (0.142)
tetra ud (3)	**4.579** (0.000)	**0.115** (0.000)	−6.544 (2.255)	0.100 (0.102)
[110] crow. (4)	rlx (3)	rlx (3)	−6.396 (2.402)	0.368 (0.369)
[011] crow. uu (5)	4.897 (0.318)	0.070 (−0.046)	−7.209 (1.589)	0.145 (0.146)
[011] crow. ud (6)	4.866 (0.287)	0.064 (−0.051)	−7.346 (1.452)	0.141 (0.142)

As a final test, we investigated the case of C in fm-HS Fe, where Jiang and Carter have determined a migration barrier in a 32-atom cell.[34] They found that the ⟨110⟩ crowdion site is an intermediate site for C migration, lying only 0.01 eV below the transition state energy and 0.98 eV above the stable octa site. Our calculations in a 32-atom cell agree well with this finding, with an energy difference of 1.01 eV between the ⟨110⟩ crowdion and octa sites for C. However, when we repeated the calculations in a 256-atom cell, we found that a configuration with C in the ⟨110⟩ crowdion was structurally unstable and spontaneously transformed as a result of the nonisotropic stress on the Fe lattice. By contrast, the isotropic stress from an octa-sited C only led to local relaxation of the Fe matrix and maintenance of the crystal structure. We conclude that the 32-atom cell effectively imposed artificial constraints that allowed a seemingly sensible migration barrier to be determined.

Overall, we find that the finite size effects in the 32-atom cell are too significant and while some intermediate cell size between the two investigated here may be sufficient, we have performed our migration energy calculations in the 256-atom cell.

1. *Interstitial He migration*

The migration of interstitial He is relevant in the initial stages after He production by transmutation and α-particle irradiation and at sufficiently high temperatures for He to escape from defect traps. The migration of He between adjacent tetra sites (that is, between sites at 1 nn on the

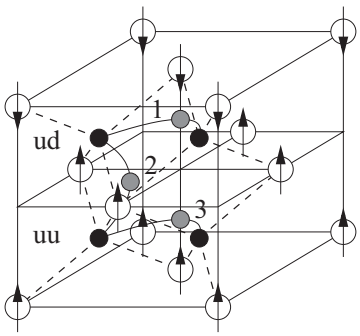

FIG. 2. Possible migration paths for interstitial He in the afmD Fe lattice. Paths are shown for 1 nn jumps from initial to final tetra positions (black circles) via off-center octa intermediate transition state positions (gray circles). The Fe atoms (white circles) are shown with arrows to indicate the local moments. The symmetry of the afmD state leads to two distinct tetra sites (uu and ud) and three distinct 1 nn jumps, as shown. In the afmI state paths 1 and 3 are equivalent but still distinct from path 2. Coordinate axes are as in Fig. 1.

cubic sublattice of tetra sites) can proceed along many distinct paths, with their corresponding transition states defining the energy barrier for the transition. A direct path would lead to an intermediate state with He in the crowdion position but the energy differences to the tetra configurations (in Tables I and III) suggest that the direct path is not the MEP and that the transition state has He in an off-center position. We show representative paths for the three distinct 1 nn jumps in afmD Fe in Fig. 2.

We have performed NEB calculations for He migration in Fe along these paths and show the formation energy difference to the most stable interstitial configuration against a suitably chosen reaction coordinate in Fig. 3, with the corresponding migration barrier heights given in Table VII. It is immediately

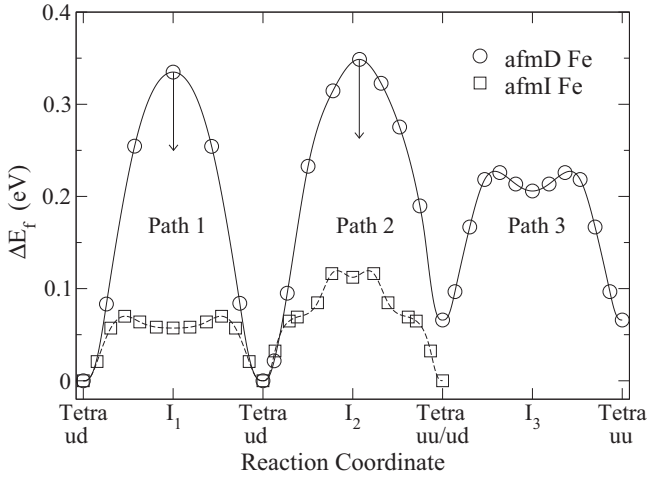

FIG. 3. Formation energy difference, ΔE_f, to the lowest energy tetra configuration along the distinct migration paths for interstitial He in Fe, as shown in Fig. 2. Positions of the tetra configurations and the intermediate configurations, I_i, along path i are labeled. In the afmI state, the data for path 3 has been omitted as it is equivalent to path 1. The arrows indicate the expected lowering of the migration barrier heights if a reorganization of magnetic moments is allowed along the migration path.

TABLE VII. Migration energy barrier height, E_m, in eV, for the migration of interstitial He along the distinct paths identified in Fig. 2. In afmD Fe, path 2 is asymmetrical and the direction of migration has been identified by the initial and final tetra sites. In Ni, all paths are equivalent and the migration energy is given by the formation energy difference between the octa [110] and tetra He configurations from Tables II and III.

Path, i	afmD Fe	afmI Fe	Ni
1	0.335	0.070	0.129
2 (ud to uu)	0.349	0.119	–
2 (uu to ud)	0.283	–	–
3	0.160	–	–

obvious that the results for the two Fe reference states differ significantly. This is not surprising, however, given that typical magnetic effects can be of the same order of magnitude as the migration barrier height (see Table I). The high barriers along paths 1 and 2 in afmD Fe are because the lowest energy tetra site is between layers of unlike moment and so not adjacent to the lowest energy octa intermediate site, which lies off-center between like-spin layers (Table III). A wholesale reorganization of spins would lower the barriers along these paths and would be preferred in the paramagnetic state. This problem is not present for path 3, resulting in a significantly lower barrier, which is more consistent with those found in the afmI state, where a more uniform distribution of energies around the octa site exists (see Table III). Path 1 in the afmI state and path 3 in the afmD state both show a double-peaked structure with weakly stable octa [001] and octa [00$\bar{1}$] intermediate states, respectively. These intermediates are equidistant from four tetra sites, resulting in the same energy barrier for 1 nn and 2nn jumps on the tetra sublattice. The same cannot be said for migration along path 2, which proceeds via a (near-)octa [110] transition state in both reference states. In the afmI state, there appears to be a very shallow minimum at I_2, that is the off-center octa [110] configuration, but with a depth of 0.007 eV this may well be just an artifact of the convergence criteria as it is less than the expected error for formation energy differences. The data also exhibits a shoulder between the tetra ud and I_2 sites, which we suggest results from close proximity to the octa [111] configuration. It seems reasonable to suggest that the barriers for 2nn jumps that cross a magnetic plane will be close in energy to those for path 2, given the additional data in Table III. Overall, our findings suggest an energy barrier for interstitial He migration in austenite that is below 0.35 eV and more likely in the region between 0.1 and 0.2 eV.

Such low migration barriers are typical of all metals for which data are available. *Ab initio* calculations find a value of 0.10 eV for fcc Al (Ref. 23), 0.07 eV for fcc Pd (Ref. 24), and 0.06 eV for bcc Fe (Ref. 25), W (Ref. 27), and V (Ref. 30). Experimental validation of these results is not forthcoming, primarily due to the low temperatures involved and the complications of He interactions within the material. In bcc W, Wagner and Seidman[75] estimate the migration enthalpy to be between 0.24 and 0.32 eV, with He being immobile up to temperatures of at least 90 K, which is consistent with the value of 0.28 eV found for ^{3}He migration by Amano and Seidman.[76] The discrepancy between *ab initio* and experiment

was explained by Becquart and Domain as being due to the presence of strong He-He binding, as found in their *ab initio* calculations, resulting in the formation of less mobile interstitial He clusters for all but the lowest concentrations.[27] This is consistent with the work of Soltan *et al.*,[77] who found He to be mobile in W and Au at temperatures below 5 K but with increasing suppression of mobility as a function of He concentration.

To this data we add the results of our own investigation into He migration in Ni. Following on from the results in afmD and afmI Fe, we make the reasonable assumption that the most stable off-center octa He configuration is a good candidate for the transition state for interstitial He migration. The additional uncertainty on the inferred migration barrier height from this assumption should be less than 0.01 eV. From the results presented in Table III this is the off-center octa ⟨110⟩ configuration, with a corresponding migration barrier height of 0.13 eV, which compares well with the experimental value of 0.14 ± 0.03 eV measured by Philipps and Sonnenberg,[78] corresponding to a migration activation temperature of 55 ± 10 K. This barrier height also compares well with our best estimate for austenitic Fe. We therefore tentatively suggest that the barrier height for interstitial He migration in austenitic Fe-Ni-based alloys will be in the range 0.1 to 0.2 eV, resulting in free, three-dimensional diffusion well below room temperature. We accept that there is a very real possibility of significant local composition dependence in these concentrated alloys but we speculate that the effective barrier height will still be in the given range.

2. Substitutional He migration

The diffusion of substitutional He generally proceeds via the dissociative and vacancy mechanisms.[7,13,79] Direct exchange with a neighboring solute atom provides an alternative mechanism[79] but is highly unlikely to contribute significantly to diffusion due to the large activation energy for the process. For example, our best estimate of the barrier height in Ni is 3.50 eV, which compares well with that found using an embedded atom model (EAM) potential of 3.1 eV by Adams and Wolfer[79] and means that substitutional He is, essentially, immobile.

For many applications, substitutional He is best considered as an interstitial He atom strongly bound to a vacancy point defect, with a binding energy, $E_b(\mathrm{He^I},\mathrm{V})$. The dissociative mechanism for substitutional He migration proceeds by the dissociation of He from a vacancy followed by interstitial migration until it becomes trapped in another vacancy. As such, the diffusion coefficient by this mechanism is inversely proportional to the vacancy concentration.[7,8,79] If thermal vacancies dominate, the activation energy is given by[7,8,13,79]

$$E_A^{\mathrm{diss.}} = E_m(\mathrm{He^I}) + E_b(\mathrm{He^I},\mathrm{V}) - E_f(\mathrm{V}), \tag{5}$$

where $E_m(\mathrm{He^I})$ is the migration energy for interstitial He. However, if there is a supersaturation of vacancies, for example, under irradiation, then the diffusion is dominated by the dissociation step and

$$E_A^{\mathrm{diss.}} = E_m(\mathrm{He^I}) + E_b(\mathrm{He^I},\mathrm{V}), \tag{6}$$

which is, essentially, the dissociation energy for substitutional He from its vacancy, and the diffusion coefficient will remain inversely proportional to the vacancy concentration.[8,79]

The diffusion of a substitutional solute by the vacancy mechanism in an fcc lattice is usually well described by the five-frequency model of Lidiard and LeClaire.[80,81] A key assumption of this model is that when a vacancy binds at 1 nn to a substitutional solute, the solute remains on-lattice. However, this is not the case for He, which we find relaxes to a position midway between the two lattice sites to form a V_2He complex. The possibility of solute-vacancy exchange at 2nn is also not included in this model, a point to which we return in the following discussion.

Given the strong binding between a vacancy and substitutional He at 1 nn, which we discuss in Sec. IV A, we assume that the migration of the V_2He complex, as a single entity, dominates the diffusion by the vacancy mechanism,[82] with a migration energy, $E_m(\mathrm{V_2He})$. The diffusion coefficient will be proportional to the V_2He concentration, which is, in turn, proportional to the vacancy concentration and depends on the binding energy between a substitutional He and a vacancy, $E_b(\mathrm{He^S},V)$. The resultant activation energy for substitutional He migration by the vacancy mechanism is given by[7]

$$E_A^{\mathrm{vac.}} = E_m(\mathrm{V_2He}) - E_b(\mathrm{He^S},V) + E_f(\mathrm{V}) \tag{7}$$

when thermal vacancies dominate and by

$$E_A^{\mathrm{vac.}} = E_m(\mathrm{V_2He}) - E_b(\mathrm{He^S},V) \tag{8}$$

when there is a supersaturation of vacancies.[25]

We have determined the migration energies for the V_2He complex using a combination of NEB and single configuration calculations. In afmD and afmI Fe, where more than one distinct V_2He complex exists, we have calculated the migration energy along all of the distinct paths where the migrating Fe atom retains the sign of its magnetic moment. In previous work,[54] we found unrealistically high migration barriers along paths where the moment changed. We label the migration paths for V_2He migration by the initial and final configurations, which are defined in Fig. 4, and present the corresponding migration energies in Table VIII.

The migration energies lie approximately 0.2 eV higher than those for the corresponding single vacancy migration in afmD and afmI Fe (Ref. 54) and in Ni, where we found a vacancy migration energy of 1.06 eV, in good agreement with other DFT calculations[22,53] and with the experimental average value[83] of 1.04 ± 0.04. We suggest that this results from the additional energy required to move the He atom from its central position in the V_2He complex back towards the lattice site during migration, as observed in all cases. We also contrast these results with those for divacancy migration. In afmD Fe, afmI Fe, and Ni we find migration energies for the divacancy along the 1b → 1b path of 0.370, 0.221, and 0.473 eV, respectively, which are significantly lower than those for the V_2He complex. In this case the difference arises not only from the energy required to move He to an on-lattice site during migration but also from its hindrance of the migrating Fe atom.

Vacancy-He exchange at 2nn provides an alternative migration path for substitutional He to that of V_2He migration. We found energy barriers for 2nn exchange as low as 0.47 and

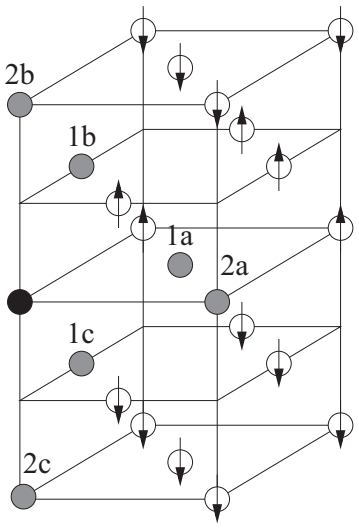

FIG. 4. Configurations for A-B pairs of interacting substitutionally sited solutes and defects in afmD Fe. Species A is shown in black and species B in gray along with the configuration label. Fe atoms are shown in white with arrows to indicate the local moments. Coordinate axes are as in Fig. 1.

0.55 eV in afmD and afmI Fe, respectively, and a value of 0.94 eV in Ni. While these results are lower than the migration energies for V_2He, the repulsive interactions between a vacancy and substitutional He at 2nn (see Sec. IV A) mean that the equilibrium concentrations of such configurations will be significantly lower than the V_2He concentration, resulting, we believe, in a much lower contribution to total diffusion. While this does strengthen our position that V_2He migration dominates substitutional He diffusion by the vacancy mechanism, a model including all the relevant migration paths is necessary to answer this question conclusively.

Using the results presented here and in Sec. IV, we evaluate the expressions in Eqs. (5)–(8) and present the results in Table IX.

The results clearly differentiate between the two mechanisms and show a strong correlation to corresponding results in bcc Fe (Ref. 25). When thermal vacancies dominate we predict that diffusion will proceed predominantly by the dissociative mechanism. If a supersaturation of vacancies exists then the vacancy mechanism clearly has the lowest activation energy. However, the vacancy concentration also plays a critical role in determining which mechanism dominates through the distinct way it enters the expressions for the diffusion coefficients. For sufficiently low but still supersaturated vacancy concentrations the dissociative mechanism may become dominant. This is, however, most likely to be the case at low temperatures

TABLE VIII. Migration energies, $E_m(V_2He)$, in eV, for the V_2He complex. The migration paths are labeled by the initial and final configurations, as defined in Fig. 4.

Path	afmD Fe	afmI Fe	Ni
1b → 1b	1.033	as 1c → 1c	1.197
1c → 1c	0.910	0.898	–
1a → 1b	1.216	–	–
1b → 1a	1.211	–	–

TABLE IX. Activation energies for substitutional He migration, in eV, by the dissociative, $E_A^{diss.}$, and vacancy, $E_A^{vac.}$, mechanisms for thermal [Eqs. (5) and (7)] and supersaturated [Eqs. (6) and (8)] vacancy concentrations. For afmD and afmI Fe we give the range of possible values corresponding to the distinct migration paths in these states.

	afmD Fe	afmI Fe	Ni
$E_A^{diss.}$, Eq. (5)	0.599–0.788	0.853–0.902	1.405
$E_A^{diss.}$, Eq. (6)	2.411–2.600	2.810–2.859	2.756
$E_A^{vac.}$, Eq. (7)	2.066–2.413	2.232–2.251	2.192
$E_A^{vac.}$, Eq. (8)	0.254–0.601	0.275–0.294	0.841

where diffusion by either mechanism is likely to be negligible. As such, we suggest that vacancy-mediated diffusion is the most important mechanism in conditions of vacancy supersaturation.

For the case of Ni, Philipps, and Sonnenberg[6] find an activation energy for He diffusion of 0.81 ± 0.04 eV from isothermal, He-desorption spectrometry experiments. They attribute this result to the diffusion of substitutional He by the dissociative mechanism, hindered by thermal vacancies, from which they infer an energy for dissociation of He of 2.4 eV. Our results agree that substitutional He migration will proceed by the dissociative mechanism in a thermal vacancy population. There is, however, a 0.6-eV difference between our calculated activation energy (Table IX) and experiment. We also find a dissociation energy for He from the substitutional site of 2.756 eV, which is in excess of the inferred experimental value. This large discrepancy suggests that the inferred experimental mechanism may not be correct. *Ab initio* calculations show that interstitial He atoms bind strongly to one another in Ni (Ref. 22). As discussed earlier, just such a mechanism was responsible for the suppression of interstitial He migration in W and may also explain the experimental result in Ni. Alternatively, the He bombardment used in the experimental setup may have resulted in a supersaturation of vacancies, in which case our calculated activation energy, at 0.84 eV, would be in good agreement with experiment.

3. *Interstitial C and N migration*

The migration of interstitial C and N in both Fe and Ni goes from octa site to adjacent octa site. In afmD Fe, there are three distinct migration paths, depending on where the initial and final octa sites lie. We label these as "in-plane," when the octa sites lie in the same magnetic plane, "uu," when the octa sites lie in adjacent magnetic planes with the same sign of magnetic moment and "ud," when the octa sites lie in adjacent magnetic planes with the opposite sign of magnetic moment. In afmI Fe, only the in plane and ud paths are distinct and in Ni, all paths are equivalent. Each of these distinct migration paths will be symmetrical about an intermediate state lying in the plane that bisects the direct path between the two octa sites. In what follows, we consider the tetra and ⟨110⟩ crowdion sites as candidate intermediate states. Possible migration paths for in-plane migration in afmD Fe are shown in Fig. 5, as an example.

For C, the results in Tables I and II show that the crowdion configurations are the lowest lying of the possible intermediate

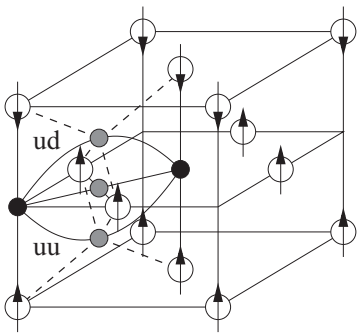

FIG. 5. Possible migration paths for interstitial C and N in afmD Fe. Paths are shows for migration from initial to final octa sites (black circles) lying in the same magnetic plane via tetra ud, [110] crowdion, and tetra uu intermediate sites (gray circles). Fe atoms (white circles) are shown with arrows to indicate the local moments. Migration between octa sites in adjacent magnetic planes have not been show for clarity. Coordinate axes are as in Fig. 1.

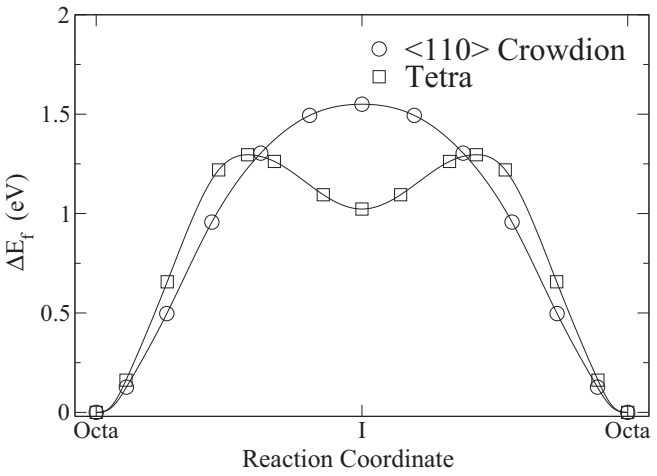

FIG. 6. Formation energy difference, ΔE_f, to the lowest energy octa configuration for N migration in Ni via tetra and ⟨110⟩ crowdion intermediate states.

states. We have performed NEB calculations in afmD Fe for C migrating from the octa site to all of the distinct crowdion sites in order to determine the energy profiles along these paths. We find a single maximum in the energy at the crowdion configurations. We find this is also the case for N migration via the crowdion configuration in Ni, as discussed below. On this basis and given the significant local dilatation necessary to form a crowdion, we make the assumption that there will be a single energy maximum at all ⟨110⟩ crowdion sites so that the MEPs and barrier heights for C migration in afmD and afmI Fe and in Ni can be determined from the data in Tables I and II. The same can also be said for N migration in afmD Fe along uu and ud paths. For all other cases, however, the tetra sites are lower in energy and we have performed NEB calculations with climbing image[84] to investigate the migration energy profiles along these paths.

In afmD Fe, our calculations confirm that the tetra ud site is the energy barrier for N migration. In afmI Fe, however, there is evidence of a shallow minimum, 0.015 eV deep, around the tetra configuration. Results in Ni, by contrast, show a clear double-peaked structure in the energy profile. We present the results in Fig. 6 and include the results for migration via the crowdion site for comparison. The results show that the tetra N configuration is a stable local minimum, with a depth of 0.273 eV relative to the transition state, and not a saddle point, like the crowdion configuration. Despite this, the MEP for N migration is still via the tetra site.

We summarize our results for the energy barriers and MEPs for interstitial C and N migration in Table X. In the Fe reference states there is a significant spread in the migration barrier heights for C migration, both along distinct migration paths and between the two states. In-plane migration clearly exhibits a higher energy barrier in both states, which results directly from the tetragonal distortion of the lattice and the subsequently higher energy necessary to form the [110] crowdion transition state. The data also suggests a significant dependence on the local magnetic order, just as was seen for interstitial He migration. The large spread in barrier heights means we cannot make any definitive predictions, except that diffusion is three-dimensional. However, in any thermodynamic average, the lower-energy paths will dominate, which suggests an effective barrier height around 1.4 eV in afmD Fe and 2.1 eV in afmI Fe. The afmD Fe value is reasonably consistent with the experimentally determined activation energies for C migration in austenite of 1.626 eV (Ref. 85) and 1.531 eV (Ref. 86).

In Ni, we find that C migrates via the crowdion site with an energy barrier height of 1.63 eV. This contrasts with the 32-atom cell, where the tetra pathway is preferred.[74] Once again, this demonstrates the inadequacy of using a 32-atom cell for solute migration in fcc Fe and Ni. Experimental results, using a variety of techniques applied both above and below the Curie temperature, $T_C = 627$ K, for Ni, yield activation energies in the range 1.43 to 1.75 eV (Ref. 87), consistent with our results. The experimental results also suggest that the influence of magnetism on the migration barrier (and enthalpy of solution) for C is no more than 0.2 eV and suggests this is the likely error in using fm Ni results to estimate those in the paramagnetic state.

Experimental results for C in Fe-Ni austenitic alloys, as discussed by Thibaux *et al.*,[88] show only slight changes in C mobility as a function of Ni composition in the range from 20 to 100 wt% Ni. They also report an activation energy of 1.30 eV in an Fe-31 wt% Ni austenitic alloy. Overall, our results, in conjunction with the experimental results we have discussed, suggest that the migration energy barrier for C migration will lie in the range 1.5 ± 0.2 eV across the whole composition range for Fe-Ni austenitic alloys.

For N, the migration barrier lies between 1.38 and 1.60 eV in afmD Fe, with a value of 1.90 eV in afmI Fe. As with C, the afmD Fe results are, on average, lower than those for the afmI state. The result of an Arrhenius fit to combined experimental diffusion data for N migration in austenite gave a similar value of 1.75 eV (Ref. 87). In Ni, we find a barrier height of 1.30 eV, which is in excess of the experimental activation energy reported by Lappalainnen and Anttila[89] of 0.99 ± 0.12 eV. In light of the significant variation in experimental results for C migration in Ni, these two results are in reasonable agreement and certainly to within the 0.2 eV we have suggested earlier as a likely error when using ferromagnetic Ni to model the

TABLE X. Migration energy barrier heights, E_m, in eV for interstitial C and N migration in afmD and afmI Fe and in Ni. Migration is between adjacent octa sites via a transition state/intermediate (TS/I), which is specified in the table, along all of the distinct paths for each particular reference state. Where the transition state/intermediate is only an intermediate state on the migration path, its name has been marked with an asterisk.

	C migration						N migration					
	afmD Fe		afmI Fe		Ni		afmD Fe		afmI Fe		Ni	
Path	E_m	TS/I	E_m	TS/I	E_m	TS/I	E_m	TS/I	E_m	TS/I	E_m	TS/I
in plane	2.033	[110] crow.	2.445	[110] crow.	1.628	⟨110⟩ crow.	1.558	tetra ud	1.899	tetra*	1.296	tetra*
uu	1.443	[011] crow. uu	as ud		as in plane		1.602	[011] crow. uu	as ud		as in plane	
ud	1.310	[011] crow. ud	2.113	[011] crow. ud	as in plane		1.384	[011] crow. ud	1.899	tetra*	as in plane	

paramagnetic state. Overall, these results show that N migrates with a significantly lower barrier in Ni than in austenitic Fe and we would expect to find an intermediate value in Fe-Ni-based alloys, more generally.

C. Solute-solute interactions

We have performed calculations to investigate the interactions between pairs of He atoms in substitutional and tetra sites in afmD and afmI Fe. Configurations with single substitutional and tetra-sited He atoms at up to 2 nn separation were found to consistently relax to a vacancy containing two He atoms. While this does not yield any useful binding energy data it does indicate that there is little or no barrier for this process and places a lower limit on the capture radius of a substitutional He of around 3 Å. Results for pairs of interacting substitutional and tetra-sited He atoms, as identified in Figs. 4 and 7, respectively, are given in Table XI.

Substitutional He pairs show consistent results across the Fe reference states with a strong positive binding at 1 nn and slightly repulsive interactions at 2 nn (Table XI). In our calculations, He atoms at 1 nn relax directly towards one another by between 0.38 and 0.44 Å, resulting in a consistent He-He separation of between 1.67 and 1.69 Å. While still close to the lattice sites, these displacements are in stark contrast to the insignificant displacements observed at 2 nn. Substitutional He pairs in Ni are similar: At 1 nn the He atoms are displaced towards one another by 0.37 Å to a He-He separation of 1.75 Å.

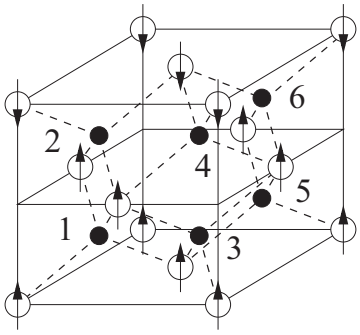

FIG. 7. Configurations for interacting tetra-sited solutes in afmD Fe. Configurations are labeled by the indices attached to the appropriate solute atom positions, shown in black. Fe atoms are shown in white with arrows to indicate the local moments. Coordinate axes are as in Fig. 1.

The resultant binding energy, at 0.657 eV, is less than in Fe but is in similar proportion to the substitutional He to vacancy binding energy (see Sec. IV A). At 2 nn He remains on-lattice with a repulsive binding energy of −0.16 eV.

Pairs of tetra-sited He atoms exhibit significant binding energies of up to 0.7 eV in afmD Fe and 0.6 eV in afmI Fe. Such strong interactions are consistently observed in bcc and fcc metals. Previous *ab initio* calculations found binding energies of 0.47 eV in Ni (Ref. 22), 0.7 eV in Pd (Ref. 24) and Al (Ref. 23), 0.4 eV in bcc Fe (Ref. 25), and 1.0 eV in W (Ref. 27). At 1 nn separation, the He atoms in afmD and afmI Fe are displaced from the tetra sites only slightly under relaxation. The resulting He-He "bonds" all lie along one of the axes of the unit cell with lengths in a small range from 1.62 to 1.68 Å, which is consistent with those found for substitutional He pairs at 1 nn. At 2 nn and 3 nn the He atoms displace significantly towards one another under relaxation from the

TABLE XI. Formation and binding energies in eV for interacting pairs of He atoms in substitutional (S) and tetra (T) sites in afmD and afmI Fe. The configurations are labeled as in Figs. 4 and 7 for S-S and T-T pairs, respectively. In the afmD reference state the binding energies between tetra-sited pairs of He atoms have been calculated relative to two isolated tetra ud He. For interacting pairs of tetra-sited He atoms at 2 nn and 3 nn separation the configurations are labeled by the initial He positions, which due to the significant displacements under relaxation should not be taken as the final positions. Eshelby corrections for S-S pairs were found to be negligible but were −0.09 eV for T-T pairs with a resulting increase in the T-T binding energies of up to 0.05 eV.

	afmD Fe		afmI Fe	
A-B/Config.	E_f	E_b	E_f	E_b
S-S/1a	7.115	0.934	7.423	0.946
S-S/1b	7.112	0.937	as S-S/1c	
S-S/1c	6.976	1.073	7.419	0.950
S-S/2a	8.197	−0.149	8.570	−0.201
S-S/2b	8.109	−0.060	8.493	−0.123
T-T/1-2	8.614	0.313	9.692	0.242
T-T/1-3	8.831	0.096	as T-T/2-4	
T-T/2-4	8.215	0.712	9.463	0.472
T-T/1-4	rlx T-T/2-5		9.403	0.531
T-T/1-5	8.700	0.227	as T-T/2-6	
T-T/2-6	8.643	0.284	9.428	0.506
T-T/2-5	8.487	0.440	9.340	0.594

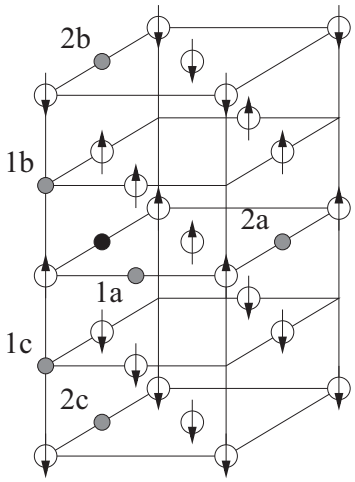

FIG. 8. Configurations for A-B pairs of interacting octa-sited interstitials in afmD Fe. Species A is shown in black and species B in gray along with the configuration labels. Fe atoms are shown in white with arrows to indicate the local moments. The lowest symmetry afmD state is shown to uniquely identify all of the distinct configurations. Some of these configurations will be symmetry equivalent in the afmI state. Coordinate axes are as in Fig. 1.

initial tetra sites, resulting in He-He separations from 1.51 to 1.65 Å. These displacements are sufficiently large to take the He atoms either to the edge of their initial tetrahedral regions or into the adjacent octahedral region via one of the faces of the tetrahedron. This is most pronounced for the 3 nn T-T/2-5 configuration, which in afmI Fe relaxed to a configuration with the He atoms within the octahedral region and symmetrically opposite the central position along the [111] axis. The situation is similar for the afmD state but one He atom is significantly closer to the central position. It is worth noting that this is the most stable configuration in afmI Fe and the second most stable in afmD Fe. The large binding energies result, simply, from the cooperative dilatation of the lattice and the reduction of repulsive He-Fe interactions, which are naturally greatest when the two He atoms are in close proximity. The results at 2 nn and 3 nn separations show that the local dilatation of the lattice around a single interstitial He results in an attractive force to other interstitial He atoms up to at least 3 Å away and encourages the formation of clusters.

To investigate interstitial cluster formation further we have determined the most stable configurations with three and four He atoms in afmD and afmI Fe. For a fixed number of He atoms we found many distinct configurations with similar energies but the most stable clusters were reasonably predictable from a simple pair interaction model, given the data in Table XI. In afmD Fe, the most stable He_3 configuration found had two He atoms in a 2-4 formation (see Fig. 7) with the third occupying the nearest octa site. In afmI Fe, the most stable was an L-shaped 1-2-3 cluster. In the most stable He_4 clusters, all He atoms occupied tetra sites in a rectangular-planar formation with 1 nn edges, such as a 1-2-3-4 cluster. This is, in fact, the most stable arrangement found in afmI Fe, whereas in afmD Fe a square-planar configuration with all He atoms in tetra ud sites was the most stable. The total binding energies for the most stable clusters are given in Table XII along with results in Ni (Ref. 22).

TABLE XII. Total binding energies, in eV, for the most stable interstitial He clusters containing up to 4 He atoms. Results in Ni are from the work of Domain and Becquart.[22] Eshelby corrections were found to be −0.19 and −0.34 eV for He_3 and He_4 clusters, respectively, with corresponding increases in the binding energies of 0.14 and 0.27 eV.

Cluster	afmD Fe	afmI Fe	Ni
He_2	0.712	0.594	0.47
He_3	1.537	1.374	1.25
He_4	2.637	2.561	

The strong clustering tendency of interstitial He is clearly demonstrated by the data. Application of the Eshelby corrections only enhances this effect. The binding energy for an additional He, that is, $E_b(He_n) - E_b(He_{n-1})$, increases with n for the small clusters studied here. We would expect this, however, to plateau to an additional binding energy of around 1 eV per He atom in afmD and afmI Fe and in Ni, given that the cooperative dilatation of the lattice that gives rise to the binding happens locally. Such strong clustering can not only result in an effective reduction in interstitial He mobility as He concentration increases but is also a critical first step in the spontaneous formation of Frenkel-pair defects, as observed in gold.[90] Indeed, the most stable He_4 configurations found here show a significant displacement of the nearest Fe atom to the cluster off lattice by 0.94 Å in afmD Fe and 1.36 Å in afmI Fe. We consider this possibility further in Sec. IV B in the context of V_mHe_n clustering.

Interactions between pairs of octa-sited C and N atoms at up to 2 nn separation in afmD and afmI Fe are given in Table XIII. The interactions are, generally, repulsive at both 1 nn and 2 nn, with a reasonable consistency between the two reference states, although the repulsion is slightly stronger in the afmI state. For C, the pair binding energy is between −0.1 and −0.15 eV at 1 nn and more repulsive at 2 nn at up to around −0.2 eV. By contrast, N pairs exhibit stronger repulsion than C

TABLE XIII. Formation and binding energies, in eV, for interacting pairs of octa-sited C and N interstitials. The configurations are as labeled in Fig. 8. Eshelby corrections were −0.03 and −0.06 eV in afmD and afmI Fe, respectively, with resultant increases in the binding energy of 0.02 and 0.03 eV.

	afmD Fe		afmI Fe	
A-B/Config.	E_f	E_b	E_f	E_b
C-C/1a	−17.490	−0.104	−17.572	−0.141
C-C/1b	−17.487	−0.106	N/A	
C-C/1c	−17.559	−0.034	−17.561	−0.151
C-C/2a	−17.420	−0.174	−17.487	−0.226
C-C/2b	−17.617	0.023	−17.655	−0.058
N-N/1a	−17.010	−0.195	−17.037	−0.204
N-N/1b	−17.035	−0.170	N/A	
N-N/1c	−17.131	−0.074	−17.020	−0.221
N-N/2a	−17.054	−0.150	−17.075	−0.167
N-N/2b	−17.212	0.008	−17.172	−0.070

at 1 nn, at around −0.2 eV and weaker repulsion at 2 nn, where the binding energy is at most around −0.15 eV. Calculations for C-C pairs at up to 4 nn separation in afmI Fe found a maximal binding energy 0.02 eV. We conclude that there will be no appreciable positive binding of C-C and N-N pairs in our reference states for austenite.

Experimental determinations of C-C and N-N interaction energies in austenite are discussed in a review by Bhadeshia.[91] If quasichemical theory, which only includes 1 nn interactions, is used to interpret the existing thermodynamic data, then a pair binding energy of −0.09 eV is found for C and −0.04 eV for N. Our results for C in afmD and afmI Fe are in good agreement with this value and while we do find a repulsive interaction between N-N pairs, we find a stronger repulsion than for C, which is contrary to the results of this analysis. A more detailed analysis can be performed using Mössbauer spectroscopy data to study the distribution of C atoms in the Fe matrix, which can be compared with the results of Monte Carlo simulations to determine the solute interaction energies at 1 nn and 2 nn.[92] Such an analysis yields C-C binding energies of −0.04 eV at 1 nn and less than −0.08 eV at 2 nn and N-N binding energies of −0.08 and −0.01 eV at 1 nn and 2 nn, respectively.[92] Our results follow the same pattern for the relative strengths of repulsion but are significantly in excess of the results of this analysis. The agreement is still impressive, however, given the level of extrapolation between our two ordered magnetic states at 0 K and temperatures where paramagnetic austenite is stable.

For C in fm Ni, Siegel, and Hamilton[74] found C-C binding energies at 1 nn and 2 nn of 0.01 and −0.01 eV, respectively, using comparative DFT calculations to those performed in this work. They, furthermore, show that this negligible level of binding is consistent with the experimental estimates of the C-C pair concentration as a function of total C concentration.[93]

From the data presented above we would suggest that C-C and N-N interactions in Fe-based austenitic alloys will be repulsive at 1 nn and 2 nn, with binding energies in the range from −0.1 to −0.2 eV. We would, furthermore, expect the level of repulsion to be reduced as a function of increasing Ni concentration.

D. Interactions with substitutional Ni and Cr solutes in Fe

As an initial step in the investigation of the interactions of He, C, and N with substitutional Ni and Cr solutes in austenite we have calculated the formation energies for single substitutional Ni and Cr and present the results in Table XIV.[94] On this basis, the results of our calculations of the interactions between He, C, and N solutes and substitutional Ni and Cr solutes in afmD and afmI Fe are presented in Table XV.

TABLE XIV. Formation energies, E_f, in eV and magnetic moments, μ, in μ_B for substitutional Ni and Cr solutes in austenitic Fe. The sign of the moments indicates whether there is alignment (positive) or anti-alignment (negative) with the moments of the atoms in the same magnetic plane.

	fct afmD		fct afmI	
Config.	E_f	μ	E_f	μ
Sub. Ni	0.083	0.039	0.145	−0.301
Sub. Cr	0.263	0.843	0.061	1.120

TABLE XV. Formation and binding energies, in eV, for substitutional Ni/Cr (species A) to substitutional He, tetra He and octa C/N (species B) with configurations labeled as in Figs. 4, 9 and 10, respectively. Eshelby corrections to E_f were found to be −0.02 eV when interstitial solutes were present but negligible for all other quantities.

	afmD Fe		afmI Fe	
A-B/cfg	E_f	E_b	E_f	E_b
sub Ni-sub He/1a	4.032	0.076	4.212	0.117
sub Ni-sub He/1b	4.035	0.073	as 1c	
sub Ni-sub He/1c	4.018	0.090	4.233	0.097
sub Ni-tetra He/1b	4.496	0.051	4.979	0.133
sub Ni-tetra He/2a	4.500	0.047	5.078	0.034
sub Ni-tetra He/2d	4.480	0.067	5.062	0.050
sub Ni-octa C/1a	−8.692	−0.021	−8.717	0.006
sub Ni-octa C/1b	−8.673	−0.040	as 1c	
sub Ni-octa C/1c	−8.729	0.016	−8.643	−0.069
sub Ni-octa N/1a	−8.439	−0.080	−8.417	−0.058
sub Ni-octa N/1b	−8.432	−0.087	as 1c	
sub Ni-octa N/1c	−8.445	−0.074	−8.349	−0.126
sub Cr-sub He/1a	4.353	−0.065	4.284	−0.038
sub Cr-sub He/1b	4.358	−0.070	as 1c	
sub Cr-sub He/1c	4.433	−0.145	4.341	−0.095
sub Cr-tetra He/1b	4.609	0.118	4.883	0.145
sub Cr-tetra He/2a	4.746	−0.019	5.005	0.023
sub Cr-tetra He/2d	4.781	−0.054	5.024	0.004
sub Cr-octa C/1a	−8.647	0.114	−8.845	0.050
sub Cr-octa C/1b	−8.628	0.094	as 1c	
sub Cr-octa C/1c	−8.730	0.197	−8.826	0.030
sub Cr-octa N/1a	−8.597	0.258	−8.729	0.169
sub Cr-octa N/1b	−8.566	0.227	as 1c	
sub Cr-octa N/1c	−8.574	0.235	−8.704	0.145

In both Fe reference states, substitutional He binds weakly to Ni, by around 0.1 eV, and has a repulsive interaction with Cr of −0.1 eV. The similarity to vacancy-substitutional Ni/Cr binding is striking.[54] The similarity also extends to the local moments on 1 nn atoms surrounding the substitutional He and vacancy, as was discussed in Sec. III. These results are also consistent with Ni and Cr acting as slightly oversized and undersized solutes, respectively, when interacting with point defects in afmD and afmI Fe, as discussed previously.[54] We would expect the interactions of other transition metal solutes with substitutional He to be readily inferred from their interactions with vacancies.

Interstitial He binds weakly to Ni by, on average, 0.09 eV at 1 nn and 0.05 eV at 2 nn in the Fe reference states. We also observe weak positive binding with Cr, but only at 1 nn, where the binding energy is, on average, 0.13 eV. Closer observations of the configurations revealed that He relaxed slightly away from Ni, but toward Cr at 1 nn. Ni also remained closer to the lattice site than Cr. These geometrical results are consistent with Ni and Cr behaving as oversized and undersized solutes, respectively, despite both exhibiting binding to interstitial He, although the binding to Cr is marginally greater. The level

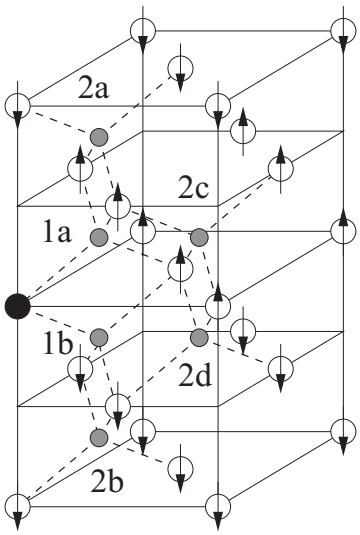

FIG. 9. Configurations for interactions between a substitutionally sited species (A) and a tetrahedrally sited species (B) in afmD Fe. Species A is shown in black, and species B is shown in gray. Configurations are labeled by the position of the tetrahedrally sited species, as shown. Fe atoms are shown in white with arrows to indicate the local moments. Coordinate axes are as in Fig. 1.

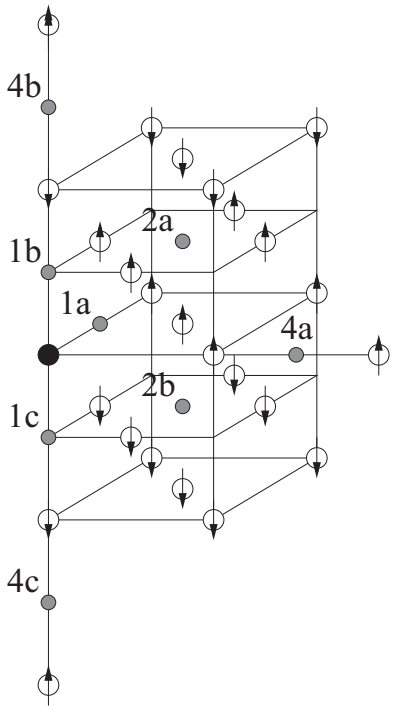

FIG. 10. Configurations for interactions between a substitutionally sited species A and octa-sited species B in the fct afmD reference state. Species A is shown in black and species B in gray along with the configuration labels. Fe atoms are shown in white with arrows to indicate the local moments. The lowest symmetry afmD state is shown to uniquely identify all of the distinct configurations. Some of these configurations will be symmetry equivalent in the afmI state. Coordinate axes are as in Fig. 1.

of binding suggests that Ni and Cr may act as weak traps for migrating interstitial He at low concentrations. However, with increasing concentration and, therefore, likelihood that He remains in similar local environments as it migrates, a direct study of the local composition dependence of the migration energy becomes necessary. From the binding energy data we can speculate, however, that such a dependence will also be weak and maintain our earlier suggestion that the activation energy for interstitial He migration will lie in the 0.1- to 0.2-eV range in concentrated Fe-Cr-Ni alloys.

The interactions of octa C and N with substitutional Ni and Cr are reasonably consistent in both afmD and afmI Fe. For C, interactions with Ni are minimal, although slightly repulsive, at 1 nn, whereas positive binding is observed with Cr on the order of 0.1 eV. The interactions of N are similar to those of C but significantly stronger and exhibit a repulsion of around −0.1 eV to Ni and attraction to Cr of around 0.2 eV. The repulsive interactions with Ni are consistent with the lower solubility of C and, particularly, N in fcc Ni, compared to afmD and afmI Fe (see Tables I and II), and suggests that the interactions are cumulative. In the case of Cr, such cumulative interactions would encourage the formation of Cr-C/N complexes and the precipitation of Cr-carbonitrides, as observed experimentally in nonstabilized austenitic stainless steels,[95] under conditions where these elements are mobile, that is, at high temperatures or in irradiated environments.

IV. SOLUTE INTERACTIONS WITH POINT DEFECTS

In this section we consider the interactions of He, C, and N with a single vacancy (V), in small vacancy-solute clusters, $V_m X_n$, and with the [001] self-interstitial (SI) dumbbell in afmD and afmI Fe and in Ni. We present the formation (and binding) energies of the underlying and most stable defects and defect clusters in Table XVI, as found previously.[54] Pairs

TABLE XVI. Formation energies, E_f, in eV, for the vacancy, the most stable di-, tri-, tetra-, and hexa-vacancy clusters, as found by Klaver *et al.*[54] and the [001] SI dumbbell in afmD and afmI Fe and in Ni. Total binding energies, E_b, in eV, are given for the vacancy clusters in brackets below the formation energies. The results in Fe are consistent with those found previously.[54] Results in Ni compare well to other DFT calculations.[21,22,53,96,97] Eshelby corrections were found to be negligible except for the tetra-vacancy in Ni at −0.03 eV, the hexavacancy at −0.06 −0.03 and −0.05 eV in afmD Fe, afmI Fe and Ni, respectively, and the dumbbell at −0.05, −0.08 and −0.10 eV in afmD Fe, afmI Fe and Ni, respectively. The only non-negligible effect on binding energies was for the hexavacancy, where increases of 0.05, 0.03, and 0.03 eV apply in afmD Fe, afmI Fe and Ni, respectively.

Defect	afmD Fe	afmI Fe	Ni
vacancy	1.812	1.957	1.352
di-vacancy	3.443	3.840	2.688
	(0.181)	(0.075)	(0.016)
tri-vacancy	4.790	5.285	
	(0.646)	(0.587)	
tetra-vacancy	6.479	7.097	4.956
	(0.768)	(0.733)	(0.451)
hexa-vacancy	8.378	9.210	6.865
	(2.493)	(2.534)	(1.245)
[001] SI dumbbell	3.196	3.647	4.135

TABLE XVII. Formation and binding energies in eV for vacancy (species A) to substitutional He, tetra He and octa C/N (species B) with configurations labeled as in Figs. 4, 9 and 10, respectively. Configurations with a single solute atom in the substitutional position (Sub.), where stable, are also considered as an interstitial solute interacting with a vacancy. In afmD Fe, the vacancy-tetra He binding energies were calculated relative to tetra ud He. Binding energies between octa C and N solutes and a vacancy at 3 nn and 4 nn separations were investigated but did not exceed 0.03 eV. The only non-negligible Eshelby corrections found were for the binding energies between a vacancy and interstitial solutes at no more than 0.02 eV in magnitude.

	afmD Fe		afmI Fe	
A-B/Config.	E_f	E_b	E_f	E_b
V-sub He/1a	5.216	0.620	5.519	0.623
V-sub He/1b	5.221	0.615	as V-sub He/1c	
V-sub He/1c	5.180	0.656	5.538	0.604
V-sub He/2a	5.940	−0.103	6.293	−0.151
V-sub He/2b	5.854	−0.018	as V-sub He/2c	
V-sub He/2c	5.919	−0.083	6.253	−0.111
V-tetra He/Sub.	4.024	2.251	4.185	2.740
V-tetra He/2a	6.328	−0.053	as V-tetra He/2b	
V-tetra He/2b	6.408	−0.133	6.932	−0.008
V-tetra He/2c	6.377	−0.101	as V-tetra He/2d	
V-tetra He/2d	6.233	0.042	6.883	0.041
V-C/Sub.	−6.981	−0.004	−6.244	−0.655
V-C/1a	−7.165	0.180	−7.276	0.377
V-C/1b	−7.040	0.056	as V-C/1c	
V-C/1c	−7.268	0.283	−7.186	0.287
V-C/2a	−7.031	0.046	as V-C/2b	
V-C/2b	−7.018	0.033	−6.948	0.049
V-N/Sub.	unstable		−5.153	−1.510
V-N/1a	−7.230	0.440	−7.275	0.612
V-N/1b	−7.065	0.275	as V-N/1c	
V-N/1c	−7.217	0.427	−7.161	0.498
V-N/2a	−6.887	0.097	as V-N/2b	
V-N/2b	−6.883	0.092	−6.769	0.106

of vacancies were consistently most stable at 1 nn separation. The most stable tetravacancy cluster consists of a tetrahedral arrangement of vacancies at 1 nn to each other. The most stable trivacancy cluster is formed from this by placing an atom near the tetravacancy center. Finally, the most stable hexavacancy is an octahedral arrangement of vacancies with 1 nn edges.

A. Vacancy-solute interactions

We present the formation and binding energies for configurations containing a single vacancy and solute atom, at up to 2 nn separation, in Table XVII.

1. V-He binding

We observe strong binding of between 0.60 and 0.66 eV for V-Sub He pairs at 1 nn in both Fe reference states. This is significantly greater than the binding between vacancy pairs[54] and represents the simplest case of enhanced vacancy binding by He, as we discuss in what follows. We find that He does not remain on-lattice at 1 nn to a vacancy but relaxes to a position best described as at the center of a divacancy. With this perspective, the V-Sub He binding represents the significant energetic preference of He for the greater free volume available at the center of a divacancy over a single vacancy. At 2 nn, the interactions are repulsive at around −0.1 eV, which is slightly greater than that observed between vacancy pairs.[54] He remains on-lattice in these configurations, which explains the lack of enhanced binding at 2 nn separation. The situation in Ni is very similar, where we find binding energies of 0.356 and −0.127 eV at 1 nn and 2 nn, respectively.

Interstitial He binds strongly to a vacancy to form a substitutional He configuration. The same is also true in Ni, where we find a binding energy of 2.627 eV, in good agreement with previous work.[22] Configurations with tetra He at 1 nn to a vacancy are unstable. At 2 nn, however, we find stable configurations with weak repulsive or attractive binding, depending on the configuration. The fact that no stable configurations were found with tetra He at up to 2 nn from a substitutional He atom demonstrates that the addition of a single He to a vacancy significantly increases the capture radius for interstitial He. We expect this effect to increase with the subsequent addition of He, given the additional pressure and dilatation that would be exerted on the surrounding lattice.

2. V-C and V-N binding

C binds to a vacancy by up to 0.38 eV at 1 nn in the Fe reference states and weakly at 2 nn. This level of binding agrees well with previous experimental and theoretical work in austenite and austenitic alloys.[47] We find that V-N binding is significantly stronger than for C with binding energies in the range from 0.3 to 0.6 eV at 1 nn and around 0.1 eV at 2 nn. For both C and N, the substitutional configuration is strongly disfavored. As discussed in Sec. III, the substitutional C and N configurations in afmD Fe were found to be unstable and the configuration labeled V-C/Sub in Table XVII has C in a stable position off lattice by 0.77 Å. Overall, these results bear a strong similarity to those found in bcc Fe (Ref. 35), where binding energies of 0.47 and 0.71 eV were found for C and N at 1 nn to a vacancy, respectively.

Results in Ni are broadly similar to those in Fe. We find a V-C binding energy of 0.062 eV at 1 nn and 0.121 eV at 2 nn. V-N binding is, again, stronger, than C, with energies of 0.362 and 0.165 eV at 1 nn and 2 nn, respectively. We also find a strong repulsion from the substitutional site. We note that the V-C binding at 1 nn seems anomalously low, given the other results but no problems were found with this calculation and other test calculations found the same stable structure and energy.

The significant V-C and V-N binding energies suggest that the relatively less mobile solutes could act as vacancy traps, much as was found in bcc Fe (Refs. 1,2,38, and 98). This would certainly be the case if dissociation of the complex was required before the vacancy could freely migrate but the possibility of cooperative migration also exists. In the fcc lattice there are many possible migration pathways that would avoid the dissociation of this complex, including some that would maintain a 1 nn separation. A complete study of these possibilities is beyond the scope of this work but preliminary calculations in Ni show that the energy barriers for C and N jumps that would maintain a 1 nn separation to the vacancy

TABLE XVIII. Total binding energies, E_b, in eV for the most stable V_mX_n clusters found in afmD and afmI Fe, where X is He, C, or N. Results in Ni are also given for C and N and can be found in the literature for He.[19,22] Eshelby corrections to E_b for V_mHe_n clusters were found to be below 0.05 eV in magnitude except for VHe_5 and V_mHe_n with m and n equal to 3 or 4, which were below 0.1 eV and VHe_6, which was 0.2 eV. For C and N clusters, the corrections were below 0.02 eV in magnitude except for those with six vacancies or with four or more N atoms, where the corrections were up to 0.1 eV for most but were 0.2 eV for VN_6 in afmI Fe and VN_5 in Ni and 0.3 eV for VN_6 in Ni.

Cluster	afmD Fe E_b	afmI Fe E_b	Cluster	afmD Fe E_b	afmI Fe E_b	Ni E_b
VHe	2.251	2.740	VC	0.283	0.377	0.121
VHe_2	3.845	4.627	VC_2	0.484	0.795	0.422
VHe_3	5.674	6.588	VC_3	0.423	0.484	−0.206
VHe_4	7.452	8.609	V_2C	0.499	0.550	0.211
VHe_5	9.239	10.305	V_4C	1.107	1.307	0.718
VHe_6	10.845	12.015	V_6C	3.546	3.253	1.531
V_2He	2.907	3.363	VN	0.440	0.612	0.362
V_2He_2	5.575	6.430	VN_2	0.981	1.295	0.872
V_2He_3	7.791	8.990	VN_3	1.264	1.341	0.877
V_2He_4	10.197	11.682	VN_4	1.371	1.514	0.933
V_3He	3.711	4.237	VN_5	1.439	1.516	0.651
V_3He_2	6.458	7.461	VN_6	1.474	1.482	0.246
V_3He_3	9.323	10.857	V_2N	0.743	0.933	0.558
V_3He_4	11.750	13.685	V_4N	1.364	1.573	1.047
V_4He	4.475	4.993	V_6N	3.224	3.466	2.033
V_4He_2	7.504	8.542				
V_4He_3	10.565	12.120				
V_4He_4	13.606	15.711				
V_6He	6.566	7.191				

are around half the value for the isolated solutes at around 0.75 eV. In contrast, vacancy jumps that maintain a 1 nn separation were found to be significantly higher than those for the isolated vacancy but jumps from 1 nn to 2 nn separation and back exhibited lower or comparable energy barriers. While these calculations are preliminary, they do indicate the distinct possibility of cooperative vacancy-solute motion that would avoid dissociation of the complex. The implications for an absence of vacancy pinning and for the enhanced diffusion of C and N solutes in the presence of vacancies in austenitic alloys makes this an interesting subject for further study.

B. Vacancy-solute clustering

Small-vacancy-He (V_mHe_n) clusters have been found to be highly stable both experimentally[8,9,11,12] and using DFT techniques[19,22–25,28] in a number of metals and are, therefore, critically important as nuclei for void formation. Experimental evidence in bcc Fe[1,2] has also shown that C can act as a vacancy trap through the formation of small, stable V_mC_n clusters, which has been confirmed in a number of DFT studies.[31,35–38] Small V_mN_n clusters have also been shown to exhibit similar stability.[35]

In this section we present the results of a large number of DFT calculations to find the most stable V_mX_n clusters, where X is He, C, or N, in afmD and afmI Fe. A comprehensive search for the most stable configuration was only practicable for the smaller clusters. For larger clusters, a number of distinct initial configurations, based around the most stable smaller clusters, were investigated to improve the likelihood that the most stable arrangement was found. The total binding energies for the most stable configurations can be found in Table XVIII.

1. V_mHe_n clusters

The geometries of the relaxed V_mHe_n clusters were constrained by the tendency to maximize He-He and He-Fe separations within the available volume and, therefore, minimize the repulsive interactions. In a single vacancy we found that this led to the following structures: two He formed dumbbells centered on the vacancy with He-He bond lengths around 1.5 Å; three He formed a near-equilateral triangle with bond lengths of between 1.6 and 1.7 Å; four He formed a near-regular tetrahedron with bond lengths between 1.6 and 1.7 Å; five He formed a near-regular triangular bipyramid with bond lengths between 1.6 and 1.8 Å; and six He formed a near-regular octahedron with bond lengths between 1.6 and 1.8 Å. In clusters with more than one vacancy, a single He atom relaxed to a central position. Additional He tended to form clusters similar to those seen in a single vacancy but now around the center of the vacancy cluster. The trivacancy case is interesting because previous DFT calculations in austenite[54] found that a configuration consisting of a tetrahedral arrangement of vacancies with one Fe atom near the center of the void, which can be considered as the smallest possible stacking fault tetrahedron (SFT), was more stable than the planar defect of three vacancies with mutual 1 nn separations. The addition of a single He atom was enough to reverse the order of stability with a difference in the total binding energy of 0.8 eV in afmI Fe, in favor of the planar defect. We suggest that this result should readily generalize, with planar defects being

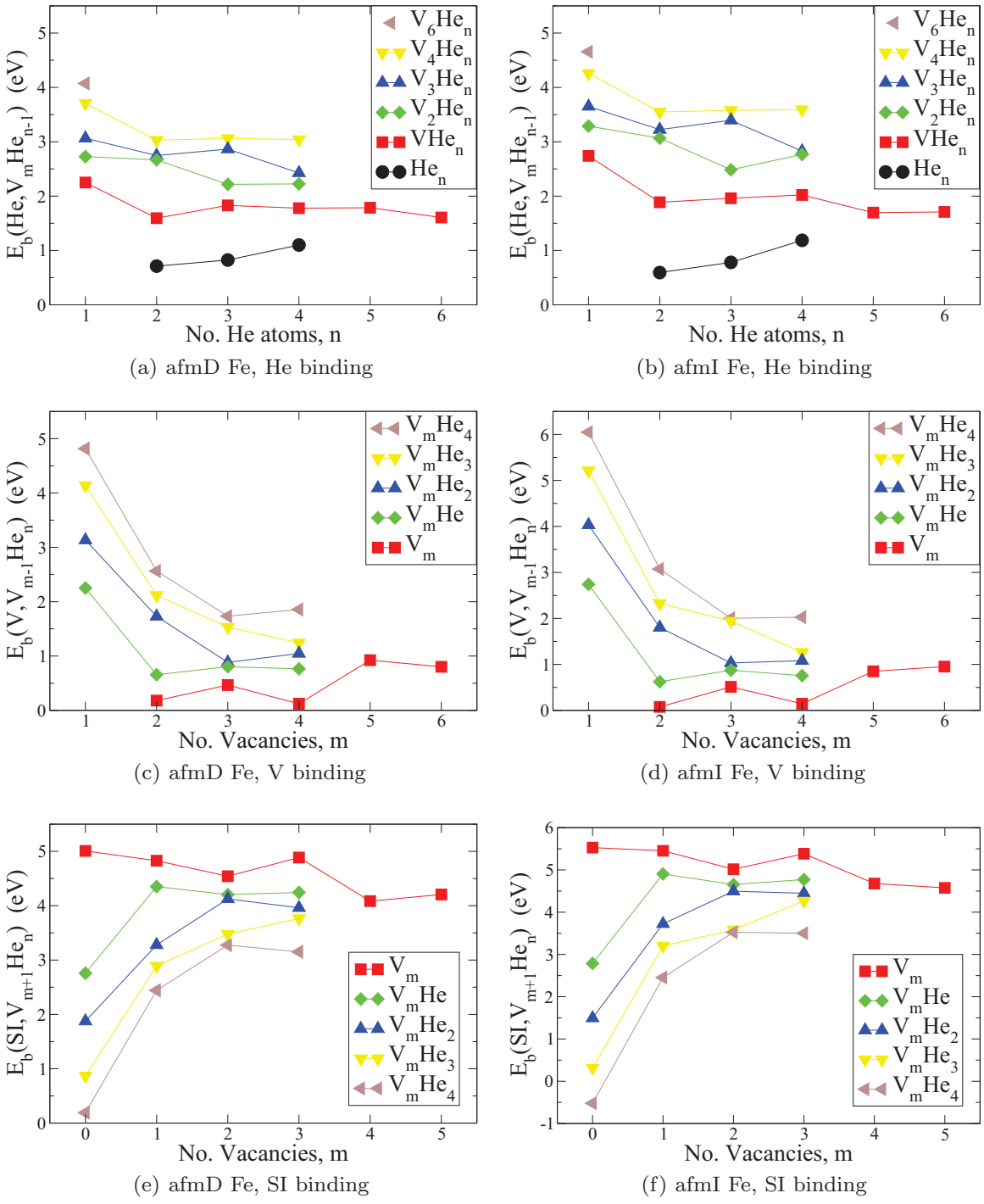

FIG. 11. (Color online) Binding energies, in eV, for a He atom, V, or SI to an existing cluster to form one with the V_mHe_n stoichiometry in afmD Fe [panels (a), (c), and (e)] and afmI Fe [panels (b), (d), and (f)] Fe. Interstitial He cluster data have been included in panels (a) and (b) for completeness.

more stable than SFTs with sufficient addition of He. That said, however, planar defects have been found[54] to be less stable than three-dimensional protovoids and this situation is unlikely to change with the addition of He due to the greater free volume of the latter clusters.

In Sec. III A1 the addition of a single He to a vacancy was found to have very little effect on the local magnetism. The addition of He to vacancy clusters was generally found to have very little effect on the total magnetic moment of the supercells containing the cluster. The only exception was for the single vacancy in afmD Fe, although it took the addition of six He atoms to significantly change the magnetic moment. Even in the absence of vacancies, a cluster of at least three He atoms was necessary to influence the total magnetic moment.

In Fig. 11 we present results for the binding energy of either a He atom, vacancy (V), or [001] self-interstitial dumbbell

(SI) to an already existing cluster to form one with the V_mHe_n stoichiometry. These results show that He consistently binds strongly to an existing cluster and that the strength of the binding only increases with m. For a fixed value of n, this binding energy will converge to the formation energy for interstitial He (see Table I) as m increases and is well on the way to doing that for $n = 1$. For fixed m the additional He binding energy appears to plateau as n increases, although it should diminish eventually as the pressure within the cluster builds.

The binding energy for an additional vacancy is also consistently positive. The presence of He significantly increases this additional binding for all values of m, which is consistent with the observation that it aids the nucleation, stabilization, and growth of voids in irradiated environments.[10,13–16] For fixed n, the data shows that the vacancy binding energy is tending to a plateau as m increases and is consistent with the fact that all of these curves should converge to the vacancy formation energy.

The SI binding energy can be related to the vacancy binding energy as

$$E_b(\mathrm{SI}, V_{m+1}He_n) = E_f(\mathrm{SI}) + E_f(\mathrm{V}) - E_b(V, V_mHe_n), \quad (9)$$

which implies that the spontaneous emission of an SI from an existing cluster will be energetically favorable if and only if the binding of the newly created vacancy is greater than the Frenkel pair formation energy. The data show that the SI binding energy clearly decreases as He concentration is increased at fixed m and for sufficiently high concentration will become negative. Indeed, it is energetically favorable for an interstitial He cluster with four He atoms in afmI Fe, and most likely for five He atoms in afmD Fe, to spontaneously emit an SI defect. This mechanism was proposed to explain the observation of He bubbles in Au samples after subthreshold He implantation[90] and could also explain observations of He trapping in Ni (Ref. 99), where the He was introduced by natural tritium decay to avoid implantation-produced defects. Our results show that this would, most likely, occur in austenite and austenitic alloys and could lead to bubble formation, with the potential for blistering in the presence of, even low-energy, bombardment by He ions, as seen in W (Refs. 100 and 101).

As a whole, the binding energy data is qualitatively similar to DFT results in Al (Ref. 23) and Pd (Ref. 24) and is quantitatively similar to results in bcc Fe (Ref. 25) and Ni (Refs. 19 and 22). This observation gives us confidence that our results are not only applicable to austenite but to austenitic alloys more generally.

The binding energy data above has also been used to determine the dissociation energy, that is the energy of emission, of He, V, or SI from a V_mHe_n cluster using the simple ansatz that the dissociation energy, $E_{\mathrm{diss.}}(X)$, for species, X, is given by

$$E_{\mathrm{diss.}}(X) = E_b(X) + E_m(X), \quad (10)$$

where $E_m(X)$ is the migration energy for isolated species, X. We present results for the dissociation energies in Fig. 12, using the migration energies in Table XIX.

There is a strong and distinct dependence on the He to vacancy ratio, n/m, for the dissociation energies of the three species. Both graphs exhibit a clear crossover between the He and V curves at around $n/m = 1.3$ and another between the He and SI curves at about $n/m = 6$. An identical He-V crossover ratio was found in bcc Fe (Ref. 25) and fcc Al (Ref. 23). For n/m below 1.3 the clusters are most prone to emission of a vacancy, between 1.3 and 6 He has the lowest dissociation energy, and above 6 SI emission is the preferred dissociation product. The slope of the curves ensures that emission of the species with the lowest dissociation energy will make the resulting cluster more stable. At sufficiently high temperatures that these processes are not limited by kinetics this should lead to the formation of the most stable clusters, which have an n/m value at the He-V crossover, where our results predict a minimum dissociation energy of around 2.8 eV in both afmD and afmI Fe.

2. V_mC_n and V_mN_n clusters

In fct afmD and afmI Fe and in Ni we considered VX_n clusters with octa-sited C and N at 1 nn to the vacancy and configurations where C and N are close enough to form C-C and N-N bonds within the vacancy. Our results for VC_2

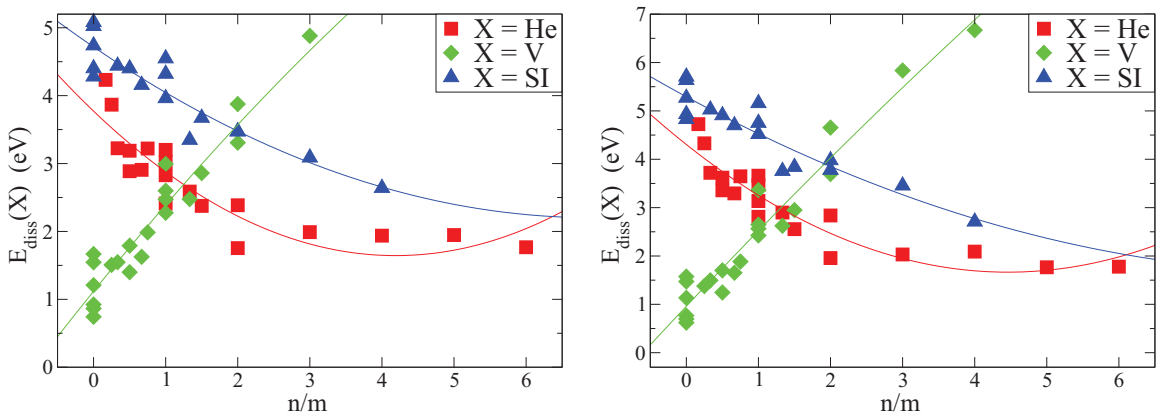

FIG. 12. (Color online) Dissociation energies, $E_{\mathrm{diss.}}(X)$, in eV, for species X from a V_mHe_n cluster, where X is a He, V, or SI. Results are presented for (a) afmD Fe and (b) afmI Fe versus the He to vacancy ratio, n/m. The solid curves are simple polynomial fits to the data and are present to aid visualization.

TABLE XIX. Migration energies, E_m(X), in eV, for species, X, where X is He, V, or SI. For He, the lowest values from Table VII were used. For V, the lowest vacancy migration energies from Klaver *et al.*[54] were used. The SI migration energies were calculated here as that for a[102] dumbbell SI migrating between two lattice sites at 1 nn separation within a magnetic plane using identical settings to Klaver *et al.*[54]

Species,X	afmD Fe	afmI Fe
He	0.160	0.070
V	0.743	0.622
SI	0.196	0.254

and VN_2 clusters are given in Table XX. We found that VX_2 clusters with octa-sited C and N are most stable when the C/N atoms are as far apart as possible, that is, opposite one another across the vacancy. For these configurations the total binding energy is more than the sum of the binding energies for each single solute to the vacancy, indicating either some chemical or cooperative strain interaction. We found that C-C dumbbells centered on the vacancy are stable, with bond lengths between 1.38 and 1.48 Å, that is, much shorter than the separations between octahedral sites. The most stable lie along ⟨100⟩ directions and binding over and above that for octa-sited C was found in afmD Fe and Ni. The enhancement in binding upon forming a C-C dumbbell is not, however, as pronounced as was seen in bcc Fe (Refs. 25 and 35–37). We also found stable configurations with N-N dumbbells in Fe and Ni with bond lengths between 1.34 and 1.49 Å, although they exhibit a much lower, and generally negative, total binding energy compared to configurations with octa-sited N atoms.

For VX_3 clusters, we investigated all possible configurations with three octa-sited C or N solutes in addition to those with a C-C dumbbell and an octa-sited C solute in one of the four octa sites perpendicular to the dumbbell axis and a configuration with three C atoms close enough for C-C bonding. Although we do find stable configurations with C-C bonding in either a dumbbell or triangular arrangement in both Fe and Ni, these arrangements are the least stable and exhibit significant, negative total binding energies. The most stable arrangements consist of three octa-sited C atoms placed as far apart as possible, for example in three 1a sites relative to the vacancy as in Fig. 10. However, the total binding energies for the most stable VC_3 clusters (see Table XVIII) are less than for VC_2, which implies that a vacancy can only bind up to two C atoms within a vacancy. A vacancy may still, however, bind more than at 2 nn octa sites but we did not investigate this possibility due to the strongest binding being at 1 nn to the vacancy and due to the large number of possible configurations.

The most stable VN_3 clusters have the same geometry as found with C but, in contrast, are more stable than VN_2 clusters. Beyond this point, we found that the total binding energy only increases for up to four N atoms in afmI Fe and Ni but increases all the way up to six N atoms in afmD Fe. That said, however, the binding energy per N atom only increases up to a VN_2 cluster in all reference states. The equilibrium concentrations of clusters with more than two N atoms, which can be calculated using the law of mass action,[38] would very likely be negligible, even at room temperature. Despite their magnitude, the Eshelby corrections do not change these conclusions but would result in the total binding energy increasing all the way up to six N atoms in afmI Fe, as was found for afmD Fe.

TABLE XX. Formation and total binding energies, in eV, for the interactions of a vacancy with two octa sited C or N solutes. Configurations with C or N in octa sites at 1 nn to the vacancy are labeled by the positions of the two solutes as in Fig. 10. When both octa solutes are in the same plane as the vacancy the configurations are additionally labeled by their relative orientation i.e. opposite (opp.) or adjacent (adj.) to one another. Doubly mixed dumbbells centered on the vacancy site were also considered as configurations of an interacting vacancy with two octa solutes and the total binding energies were calculated accordingly. Eshelby corrections to both E_f and E_b were found to be no more than 0.03 eV in magnitude.

	afmD Fe		afmI Fe		Ni	
Config.	E_f	E_b	E_f	E_b	E_f	E_b
			VC_2 clusters			
1a-1a (opp.)	−16.226	0.444	−16.551	0.795	−15.692	0.199
1b-1c	−16.166	0.385	−16.466	0.711	as 1a-1a (opp.)	
1a-1a (adj.)	−15.908	0.127	−16.163	0.408	−15.396	−0.097
1a-1b	−15.832	0.050	−16.116	0.361	as 1a-1a (adj.)	
1a-1c	−16.104	0.323	as 1a-1b		as 1a-1a (adj.)	
[100] dumb.	−16.087	0.305	−16.224	0.469	−15.915	0.422
[001] dumb.	−16.265	0.484	−16.262	0.507	as [100] dumb.	
[110] dumb.	−15.407	−0.375	−15.238	−0.517	−15.380	−0.113
[111] dumb.	rlx [001] dumb.				−15.565	0.072
			VN_2 clusters			
1a-1a (opp.)	−16.373	0.981	−16.579	1.295	−14.559	0.872
1b-1c	−16.124	0.732	−15.932	0.648	as 1a-1a (opp.)	
1a-1a (adj.)	−16.113	0.720	−16.237	0.953	−14.279	0.591
1a-1b	−16.051	0.658	−16.037	0.753	as 1a-1a (adj.)	
1a-1c	−16.228	0.835	as 1a-1b		as 1a-1a (adj.)	
[100] dumb.	−14.451	−0.942	−14.487	−0.796	−13.616	−0.071

We investigated site preference and binding for single C and N solutes to the most stable di-, tetra-, and hexavacancy clusters in afmD and afmI Fe and in Ni. For the V_2C cluster in afmD Fe, we considered all 1 nn octa sites to the three distinct types of 1 nn divacancy as well as configurations with C at the center of all 1 nn and 2 nn divacancy clusters. For the octa sites, C was found to bind to existing divacancy clusters with similar binding energies to a single vacancy, that is with $E_b(C,V_2)$ in the range from 0.03 to 0.32 eV. The most stable of these, which was also found to be the most stable V_2C cluster, contained the most stable divacancy and bound C more stably than to a single vacancy. We found that C was repelled from the center of a 1 nn divacancy lying within a magnetic plane but bound to the other two 1 nn divacancies with energies similar to those found in octa sites. As in bcc Fe (Refs. 31,36, and 37), the most preferred site for C was at the center of a 2 nn divacancy, with $E_b(C,V_2) = 0.35$ eV. However, this was not sufficient to overcome the difference in stability between 1 nn and 2 nn divacancies in afmD Fe (Ref. 54) and did not, therefore, form the most stable V_2C cluster, in contrast to in bcc Fe.

The analysis above motivated the use of only the most stable 1 nn divacancy in the remaining calculations along with configurations containing solutes at the center of 2 nn divacancies. For N in afmD Fe, the order of site preference mirrors that for C. An N solute is capable of stabilizing a 2 nn divacancy configuration but the most stable V_2N cluster shared the same geometry as for C with a binding energy to the underlying divacancy of 0.56 eV, which is, again, in excess of the binding to a single vacancy.

The situation in afmI Fe and Ni was found to be rather similar to that of afmD Fe. For both C and N, the site at the center of a 1 nn (in-plane) divacancy was disfavored. The most stable configuration generally contained an octa-sited solute bound to a 1 nn divacancy. The only exception was in afmI Fe, where a configuration with C at the center of a 2 nn divacancy lying within a magnetic plane had a greater total binding energy but only by 0.03 eV. This most likely resulted from the much smaller energy difference between 1 nn and 2 nn divacancies in afmI Fe of compared to afmD Fe (Ref. 54) and to Ni, where we find an energy difference of 0.1 eV in favor of the 1 nn divacancy. In the most stable clusters, the binding of the solutes to the underlying divacancy was, once again, in excess of the binding to a single vacancy.

For the binding of C and N to the most stable tetravacancy, we found that the central position was extremely disfavored. We investigated all configurations with solute atoms in an octa site at 1 nn to at least a single vacancy. We also performed calculations with solute atoms placed initially at random within the protovoid but found that these relaxed to octa sites already considered. Configurations with only a single vacancy at 1 nn to the solute were found to be the most stable. The total binding energies for these configurations are given in Table XVIII. Using these results we found that the binding of C and N to the tetravacancy was in excess of that to a divacancy and a single vacancy, in all cases except for N in afmI Fe, where the binding to the tetravacancy and divacancy reversed order, although they differ by only 0.02 eV.

For the hexavacancy, the central octa site was unstable for both C and N in afmD Fe. In afmI Fe and Ni it was stabilized by symmetry but still strongly disfavored. This repulsion is, however, significantly less than was observed for the tetravacancy. Closer observation showed that while the nearest neighboring Fe and Ni atoms to the solutes moved very little under relaxation in the tetravacancy, the contraction in bond length was between 25% and 30% in the hexavacancy from an initial separation of around 3 Å. This demonstrates how important the formation of strong chemical bonds with characteristic bond lengths is to the stability of configurations containing C and N in Fe and Ni.

We investigated the stability of configurations with C and N in all octa sites at 1 nn to at least one vacancy in the hexavacancy cluster. We found that there were additional stable sites, lying along ⟨100⟩ axes projected out from the center of the hexavacancy. For C, these sites were found to lie between the first vacancy reached along these axes and the next octa site out. They are close to but distinct from the octa sites and we, therefore, refer to them as octa-b sites. For N, stable sites were found between the center of the hexavacancy and the first vacancy reached along the ⟨100⟩ axes and we refer to these as off-center sites. We found that C was, consistently, most stable in an octa-b site, whereas N preferred octa sites with two vacancies at 1 nn, although an off-center site along $[00\bar{1}]$ was the most stable in afmD Fe.

Once again, the binding energy between the solutes and hexavacancy was greater than for all smaller vacancy clusters. We summarize these results for $E_b(X,V_m)$ in Fig. 13, which clearly shows the increase in binding energy as the vacancy cluster becomes larger. It also clearly shows that in the same reference state, the binding energy for N is consistently greater than for C and that the binding energies in afmI Fe lie above those in afmD Fe. The one anomalous point is the binding energy for C to a hexavacancy in afmD Fe, which is much larger than the trends would suggest. Other configurations with C in an octa-b site in afmD Fe exhibited similar levels of binding and no problems with any of these calculations or instabilities in the relaxed structures could be found.

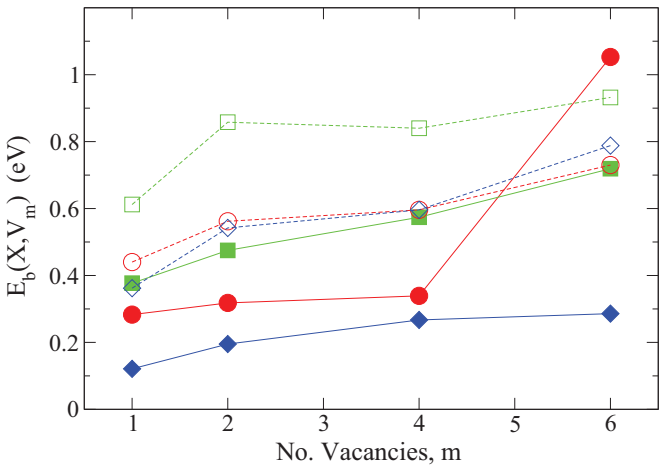

FIG. 13. (Color online) Binding energy, $E_b(X,V_m)$, in eV, where X is C (solid symbols and solid lines) or N (open symbols and dashed lines) in afmD Fe (red circles), afmI Fe (green squares) and Ni (blue diamonds). The binding energies were calculated for the most stable clusters.

TABLE XXI. Formation and binding energies in eV for [001] self-interstitial dumbbell (species A) - solute (species B) interactions. For octa-sited C and N solutes the configurations are labeled as in Fig. 10. He interactions were investigated with He sited substitutionally and tetrahedrally with configurations labeled as in Figs. 4 and 9, respectively. Configurations with substitutional He in 1b and 1c positions relative to a [001] dumbbell SI were unstable to defect recombination and interstitial He kickout. In Ni, the [001]-tetra He binding energy was observed to be 0.20 eV.[22] Eshelby corrections were found down to -0.1 eV for configurations containing substitutional He but the related increases in E_b were no more than 0.02 eV. For configurations containing interstitial solutes $E^{corr.}$ could be as low as -0.2 eV with corresponding increases in E_b up to 0.08 eV.

	afmD Fe		afmI Fe		Ni	
A-B/Config.	E_f	E_b	E_f	E_b	E_f	E_b
[001]-tetra He/1a	unstable		unstable			
[001]-tetra He/1b	7.734	−0.075	as 1a			
[001]-tetra He/2a	7.494	0.166	8.517	0.098		
[001]-tetra He/2b	7.761	−0.036	as 2a			
[001]-tetra He/2c	7.609	0.117	8.435	0.180		
[001]-tetra He/2d	7.514	0.146	as 2c			
[001]-sub He/1a	7.045	0.176	7.743	0.089	7.085	0.235
[001]-sub He/2a	7.164	0.057	7.815	0.017	7.316	0.003
[001]-sub He/2b	7.050	0.171	7.653	0.179	unstable	
[001]-sub He/2c	7.095	0.126	as 2b		as 2b	
[001]-C/1a	−5.563	−0.037	−5.007	−0.202	−4.300	0.012
[001]-C/1b	−4.604	−0.997	−3.975	−1.234		
[001]-C/1c	−4.459	−1.141	as 1b			
[001]-C/2a	−5.585	−0.015	−5.064	−0.145	−4.322	0.034
[001]-C/2b	−5.527	−0.074	as 2a		as 2a	
[001]-C/4a	−5.626	0.025	−5.266	0.057	−4.303	0.015
[001]-C/4b	−5.652	0.051	−5.287	0.078	−4.362	0.075
[001]-C/4c	−5.642	0.041	as 4b		as 4b	
[001]-N/1a	−5.106	−0.300	−4.444	−0.529	−3.198	−0.188
[001]-N/1b	−4.461	−0.945	−3.721	−1.252		
[001]-N/1c	−4.197	−1.209	as 1b			
[001]-N/2a	−5.290	−0.116	−4.762	−0.211	−3.400	0.015
[001]-N/2b	−5.251	−0.155	as 2a		as 2a	
[001]-N/4a	−5.425	0.019	−5.027	0.054	3.402	0.017
[001]-N/4b	−5.430	0.024	−5.043	0.069	−3.481	0.096
[001]-N/4c	−5.458	0.052	as 4b		as 4b	

C. [001] dumbbell SI-solute interactions

We investigated the binding of He, C, and N solutes to a [001] dumbbell in afmD and afmI Fe and in Ni and present the results in Table XXI.

We found that interstitial He, placed initially 1 nn to a [001] SI dumbbell, either spontaneously displaced under relaxation to a 2 nn site or exhibited a repulsive binding energy in Fe. At 2 nn, however, a positive binding energy was observed, up to almost 0.2 eV, as was found in Ni (Refs. 19 and 22). Eshelby corrections do not qualitatively change these results and would only act to enhance the binding at 2 nn. This positive binding energy is comparable to that in bcc Fe (Ref. 25) but while significant, it is only likely to result in mutual trapping at low temperature, given the high mobility of the two species. Taken as a model for the binding of interstitial He to other overcoordinated defect sites, such as near dislocations and grain boundaries, however, this result does show that He would be likely to be trapped at such sites, leading to interstitial He cluster formation and spontaneous bubble nucleation and growth, as discussed earlier. It is worth mentioning that bubble nucleation by this mechanism would happen much more readily at grain boundaries where, due to their disorder, vacancies can be formed without the additional SI.

A substitutional He atom in the 1b and 1c sites (see Fig. 4) to a [001] SI dumbbell resulted in the spontaneous recombination of the vacancy and SI and the kickout of an interstitial He atom. At all other 1 nn and 2 nn sites except 2b in Ni, however, stable complexes with binding energies of up to around 0.2 eV were formed. Barriers to recombination for these complexes, while positive, were not calculated in this work. These results do, however, show that substitutional He and most likely other V_mHe_n clusters can act as trapping sites for SI dumbbells in austenite and austenitic alloys with a capture radius extending out to at least 2 nn. We can also speculate that, once trapped, recombination will be likely to occur.

Both C and N are either repelled from 1 nn and 2 nn sites to a [001] SI dumbbell or show very little positive binding, much as was observed in bcc Fe (Ref. 35). Eshelby corrections do

not change this conclusion in Fe but would result in binding of around 0.1 eV at 2 nn in Ni. Motivated by the result that C does exhibit positive binding to the most stable SI and small SI clusters in bcc Fe (Ref. 19) at further separation, we investigated this possibility here and found sites with binding energies from 0.05 to 0.1 eV at 4 nn to the dumbbell, which would only be enhanced by Eshelby corrections. These sites can be related to the corresponding ones in bcc Fe by a Bain transformation[102] and the binding almost certainly results from strain field effects in both cases. The fact that such binding was found to increase with interstitial cluster size[19] means that Cottrell atmospheres[3] of C and N are very likely to form around other overcoordinated defects, such as dislocations and grain boundaries, in both ferritic and austenitic alloys under conditions where these species are mobile.

V. CONCLUSIONS

An extensive set of first-principles DFT calculations have been performed to investigate the behavior and interactions of He, C, an N solutes in austenite, dilute Fe-Cr-Ni alloys, and Ni as model systems for austenitic steel alloys. In particular, we have investigated the site stability and migration of single He, C, and N solutes, their self-interactions, interactions with substitutional Ni and Cr solutes, and their interactions with point defects typical of irradiated environments, paying particular attention to the formation of small $V_m X_n$ clusters.

Direct comparison with experiment verifies that the two-state approach used to model austenite in this work is reasonably predictive. Overall, our results demonstrate that austenite behaves much like other fcc metals and is qualitatively similar to Ni in many respects. We also observe a strong similarity between the results presented here for austenite and those found previously for bcc Fe.

We find that interstitial He is most stable in the tetrahedral site and migrates via off-center octahedral transition states with a migration energy from 0.1 to 0.2 eV in austenite and 0.13 eV in Ni. The similarity of these results and the weak interactions with Ni and Cr solutes in austenite suggests a migration energy in Fe-Cr-Ni austenitic alloys in the 0.1- to 0.2-eV range. Interstitial He will, therefore, migrate rapidly from well below room temperature until traps are encountered. Its strong clustering tendency, with an additional binding energy approaching 1 eV per He atom in austenite and 0.7 eV in Ni, will lead to a reduction in mobility as interstitial He concentration increases. Interactions with overcoordinated defects, which are on the order of a few tenths of 1 eV, will result in the buildup and clustering of interstitial He at dislocations and grain boundaries. The most stable traps, however, are vacancy clusters and voids, with binding energies of a few eV. The strength of this binding means that growing interstitial He clusters eventually become unstable to spontaneous Frenkel pair formation, resulting in the emission of a self-interstitial and nucleation of a VHe_n cluster. The binding of additional He and vacancies to existing V_mHe_n clusters increases significantly with cluster size, leading to unbounded growth and He bubble formation in the presence of He and vacancy fluxes. The most stable clusters have a helium-to-vacancy ratio, n/m, of around 1.3, with a dissociation energy for the emission of He and V of 2.8 eV in austenite and Ni. Generally, we assume that V_mHe_n clusters are immobile. For the simplest case of substitutional He, however, migration is still possible. In a thermal vacancy population, diffusion by the dissociative mechanism dominates, with an activation energy of between 0.6 and 0.9 eV in Fe and 1.4 eV in Ni. In irradiated environments, however, the vacancy mechanism dominates and diffusion can proceed via the formation and migration of the stable V_2He complex, with an activation energy of between 0.3 and 0.6 eV in Fe and 0.8 eV in Ni.

We find that C and N solutes behave similarly, both in austenite and Ni, although the interactions of N are stronger. The octahedral lattice site is preferred by both solutes, leading to a net expansion of the lattice and a reduction of the c/a ratio in the afmD and afmI Fe reference states. Both solutes also stabilize austenite over ferrite and favor ferromagnetic over antiferromagnetic states in austenite. Carbon migrates via a $\langle 110 \rangle$ transition state with a migration energy of at least 1.3 eV in austenite and of 1.6 eV in Ni. For N, migration proceeds via the crowdion or tetrahedral sites, depending on path, with a migration energy of at least 1.4 eV in austenite and 1.3 eV in Ni. Pairs of solute atoms are repelled at 1 nn and 2 nn in austenite and do not interact in Ni. Both C and N interact very little with Ni solutes in austenite but bind to Cr, which may act as a weak trap and encourage the formation of Cr-carbonitrides under conditions where the solutes are mobile. Carbon binds to a vacancy by up to 0.4 eV in austenite and 0.1 eV in Ni, with N binding more strongly at up to 0.6 eV in austenite and 0.4 eV in Ni. While this may suggest that C and N act as vacancy traps, as in bcc Fe, preliminary calculations in Ni show that VC and VN clusters may diffuse cooperatively with an effective migration energy similar to that for the isolated vacancy. This also raises the possibility of enhanced C and N mobility in irradiated alloys and their segregation to defect sinks. A vacancy can bind up to two C atoms and up to six N atoms in austenite (or four in Ni), although the additional binding energy reduces significantly above two. Covalent bonding was observed between solutes in a vacancy but did not lead to any enhanced stability, as seen in bcc Fe. Both C and N show a strong preference for sites near the surface of vacancy clusters and the binding increases with cluster size, suggesting that they will decorate the surface of voids and gas bubbles, when mobile. A binding energy of 0.1 eV was observed to a [001] SI dumbbell in austenite and Ni, which we would expect to increase with interstitial cluster size, as in bcc Fe, resulting in Cottrell atmospheres of C and N around dislocations and grain boundaries in austenitic alloys.

Along with previous work, these results provide a complete database that would allow realistic Fe-Cr-Ni austenitic alloy systems to be modeled using higher-level techniques, such as molecular dynamics using empirical potentials and kinetic Monte Carlo simulations. As such, they play a critical role in a multiscale modeling approach to study the microstructural evolution of these materials under irradiation in typical nuclear environments.

ACKNOWLEDGMENT

This work was part sponsored through the EU-FP7 PERFORM-60 project, the G8 funded NuFUSE project, and EPSRC through the UKCP collaboration.

*dhepburn@ph.ed.ac.uk
†gjackland@ed.ac.uk

[1] A. Vehanen, P. Hautojärvi, J. Johansson, J. Yli-Kauppila, and P. Moser, Phys. Rev. B **25**, 762 (1982).
[2] S. Takaki, J. Fuss, H. Kuglers, U. Dedek, and H. Shultz, Radiat. Eff. **79**, 87 (1983).
[3] A. H. Cottrell and B. A. Bilby, Proc. Phys. Soc. A **62**, 49 (1949).
[4] C. S. Becquart and C. Domain, Curr. Opin. Solid State Mater. Sci. **16**, 115 (2012).
[5] D. Edwards, Jr. and E. V. Kornelsen, Surf. Sci. **44**, 1 (1974).
[6] V. Philipps, K. Sonnenerg, and J. M. Williams, J. Nucl. Mater. **107**, 271 (1982).
[7] V. Sciani and P. Jung, Radiat. Eff. **78**, 87 (1983).
[8] R. Vassen, H. Trinkaus, and P. Jung, Phys. Rev. B **44**, 4206 (1991).
[9] A. V. Fedorov, A. van Veen, and A. I. Ryazanov, J. Nucl. Mater. **233–237**, 385 (1996); **258–263**, 1396 (1998).
[10] A. van Veen, R. J. M. Konings, and A. V. Fedorov, J. Nucl. Mater. **320**, 77 (2003).
[11] X. Z. Cao, Q. Xu, K. Sato, and T. Yoshiie, J. Nucl. Mater. **412**, 165 (2011); **417**, 1034 (2011).
[12] K. Ono, H. Sasagawa, F. Kudo, M. Miyamoto, and Y. Hidaka, J. Nucl. Mater. **417**, 1026 (2011).
[13] L. K. Mansur, E. H. Lee, P. J. Maziasz, and A. P. Rowcliffe, J. Nucl. Mater. **141–143**, 633 (1986).
[14] Y. Murase, J. Nagakawa, N. Yamamoto, and H. Shiraishi, J. Nucl. Mater. **255**, 34 (1998).
[15] L. Liu, T. Mitamura, M. Terasawa, A. Yamamoto, and H. Tsubakino, Int. J. Nano. **3**, 765 (2004).
[16] L. Peng, Q. Huang, S. Ohnuki, and C. Yu, Fus. Eng. Des. **86**, 2624 (2011).
[17] H. Schroeder, W. Kesternich, and Hans Ullmaier, Nucl. Eng. Design/Fusion **2**, 65 (1985).
[18] Y. Katoh, M. Ando, and A. Kohyama, J. Nucl. Mater **323**, 251 (2003).
[19] L. Malerba *et al*., J. Nucl. Mater. **406**, 7 (2010).
[20] http://www.perform60.net/
[21] X. T. Zu, L. Yang, F. Gao, S. M. Peng, H. L. Heinisch, X. G. Long, and R. J. Kurtz, Phys. Rev B **80**, 054104 (2009).
[22] C. Domain and C. S. Becquart, FP7 PERFECT Project Report for deliverable P58, 2007 (unpublished).
[23] L. Yang, X. T. Zu, and F. Gao, Physica B **403**, 2719 (2008).
[24] X. Zeng, H. Deng, and W. Hu, Nucl. Instrum. Methods Phys. Res., Sect. B **267**, 3037 (2009).
[25] C.-C. Fu and F. Willaime, Phys. Rev. B **72**, 064117 (2005); C.-C. Fu and F. Willaime, J. Nucl. Mater. **367–370**, 244 (2007).
[26] T. Seletskaia, Yu. Osetsky, R. E. Stoller, and G. M. Stocks, Phys. Rev. Lett. **94**, 046403 (2005).
[27] C. S. Becquart and C. Domain, Phys. Rev. Lett. **97**, 196402 (2006).
[28] C. S. Becquart and C. Domain, J. Nucl. Mater. **385**, 223 (2009).
[29] C.s. Becquart, C. Domain, U. Sarkar, A. DeBacker, and M. Hou, J. Nucl. Mater. **403**, 75 (2010).
[30] P. Zhang, J. Zhao, Y. Qin, and B. Wen, J. Nucl. Mater. **413**, 90 (2011).
[31] C. J. Ortiz, M. J. Caturla, C. C. Fu, and F. Willaime, Phys. Rev. B **75**, 100102(R) (2007); J. Nucl. Mater **386–388**, 33 (2009); Phys. Rev. B **80**, 134109 (2009).
[32] D. J. Hepburn and G. J. Ackland, Phys. Rev. B **78**, 165115 (2008).
[33] C.-C. Fu, J. Dalla Torre, F. Willaime, J.-L. Bocquet, and A. Barbu, Nat. Mater. **4**, 68 (2005).
[34] D. E. Jiang and E. A. Carter, Phys. Rev. B **67**, 214103 (2003).
[35] C. Domain, C. S. Becquart, and J. Foct, Phys. Rev. B **69**, 144112 (2004).
[36] C. J. Först, J. Slycke, K. J. Van Vliet, and S. Yip, Phys. Rev. Lett. **96**, 175501 (2006).
[37] T. T. Lau, C. J. Först, Xi Lin, J. D. Gale, S. Yip, and K. J. Van Vliet, Phys. Rev. Lett. **98**, 215501 (2007).
[38] C.-C. Fu, E. Meslin, A. Barbu, F. Willaime, and V. Oison, Solid State Phenom. **139**, 157 (2008).
[39] C. A. Wert, Phys. Rev. **79**, 601 (1950).
[40] W. R. Thomas and G. M. Leak, Phil. Mag. (Series 7) **45**, 656 (1954).
[41] V. G. Gavriljuk, V. N. Shivanyuk, and B. D. Shanina, Acta Mater. **53**, 5017 (2005).
[42] D. W. Boukhvalov, Yu. N. Gornostyrev, M. I. Katsnelson, and A. I. Lichtenstein, Phys. Rev. Lett. **99**, 247205 (2007).
[43] V. G. Gavriljuk, B. D. Shanina, V. N. Shyvanyuk, and S. M. Teus, J. Appl. Phys. **108**, 083723 (2010).
[44] N. I. Medvedeva, D. Van Aken, and J. E. Medvedeva, J. Phys.: Condens. Matter **22**, 316002 (2010).
[45] S. Kibey, J. B. Liu, M. J. Curtis, D. D. Johnson, and H. Sehitoglu, Acta Mater. **54**, 2991 (2006).
[46] A. Abbasi, A. Dick, T. Hickel, and J. Neugebauer, Acta Mater. **59**, 3041 (2011).
[47] J. A. Slane, C. Wolverton, and R. Gibala, Met. Mater. Trans. A **35**, 2239 (2004).
[48] P. Olsson, I. A. Abrikosov, L. Vitos, and J. Wallenius, J. Nucl. Mater. **321**, 84 (2003).
[49] B. Alling, T. Marten, and I. A. Abrikosov, Phys. Rev. B **82**, 184430 (2010).
[50] F. Körmann, A. Dick, B. Grabowski, T. Hickel, and J. Neugebauer, Phys. Rev. B **85**, 125104 (2012).
[51] P. Steneteg, B. Alling, and I. A. Abrikosov, Phys. Rev. B **85**, 144404 (2012).
[52] T. P. C. Klaver, P. Olsson, and M. W. Finnis, Phys. Rev. B **76**, 214110 (2007).
[53] J. D. Tucker, R. Najafabadi, T. R. Allen, and D. Morgan, J. Nucl. Mater. **405**, 216 (2010).
[54] T. P. C. Klaver, D. J. Hepburn, and G. J. Ackland, Phys. Rev. B **85**, 174111 (2012).
[55] G. Kresse and J. Hafner, Phys. Rev. B **47**, 558 (1993).
[56] G. Kresse and J. Furthmuller, Phys. Rev. B **54**, 11169 (1996).
[57] J. P. Perdew, J. A. Chevary, S. H. Vosko, K. A. Jackson, M. R. Pederson, D. J. Singh, and C. Fiolhais, Phys. Rev. B **46**, 6671 (1992).
[58] S. H. Vosko, L. Wilk, and M. Nusair, J. Can. Phys. **58**, 1200 (1980).
[59] P. E. Blöchl, Phys. Rev. B **50**, 17953 (1994).
[60] G. Kresse and D. Joubert, Phys. Rev. B **59**, 1758 (1999).
[61] M. Methfessel and A. T. Paxton, Phys. Rev. B **40**, 3616 (1989).
[62] H. Jónsson, G. Mills, and K. W. Jacobsen, in *Classical and Quantum Dynamics in Condensed Phase Simulations*, edited by B. J. Berne, G. Ciccotti, and D. F. Coker (World Scientific, Singapore, 1998), Chap. 16, p. 385.
[63] G. J. Ackland and R. Thetford, Phil. Mag. A **56**, 15 (1987).
[64] S. Han, L. A. Zepeda-Ruiz. G. J. Ackland, R. Car, and D. J. Srolovitz, J. Appl. Phys. **93**, 3328 (2003).

[65]P. Olsson, T. P. C. Klaver, and C. Domain, Phys. Rev. B **81**, 054102 (2010).
[66]N. Juslin and K. Nordlund, J. Nucl. Mater. **382**, 143 (2008).
[67]P. H. Chen, X. C. Lai, L. Z. Liu, X. L. Wang, B. Bai, B. Y. Ao, and Y. Long, J. Nucl. Mater. **405**, 156 (2010).
[68]B. D. Butler and J. B. Cohen, Ultramicroscopy **52**, 238 (1993); J. Phys. I **2**, 1059 (1992).
[69]L. Cheng, A. Böttger, Th.H. de Keijser, and E. J. Mittemeijer, Scr. Metall. Mater. **24**, 509 (1990).
[70]A. Dick, F. Körmann, T. Hickel, and J. Neugebauer, Phys. Rev. B **84**, 125101 (2011).
[71]M. A. Shumilov, A. P. Kozak, L. I. Yakushechkina, and K. N. Sokolov, Zh. Fiz. Khim. **47**, 2169 (1973).
[72]I. A. Abrikosov, A. E. Kissavos, F. Liot, B. Alling, S. I. Simak, O. Peil, and A. V. Ruban, Phys. Rev. B **76**, 014434 (2007).
[73]J. A. Lobo and G. H. Geiger, Metall. Trans. A **7**, 1359 (1976).
[74]D. J. Siegel and J. C. Hamilton, Phys. Rev. B **68**, 094105 (2003).
[75]A. Wagner and D. N. Seidman, Phys. Rev. Lett. **42**, 515 (1979).
[76]J. Amano and D. N. Seidman, J. Appl. Phys. **56**, 983 (1984).
[77]A. S. Soltan, R. Vassen, and P. Jung, J. Appl. Phys. **70**, 793 (1991).
[78]V. Philipps and K. Sonnenberg, J. Nucl. Mater. **114**, 95 (1983).
[79]J. B. Adams and W. G. Wolfer, J. Nucl. Mater. **158**, 25 (1988).
[80]A. B. Lidiard, Phil. Mag. (Series 7) **46**, 1218 (1955).
[81]A. D. LeClaire and A. B. Lidiard, Phil. Mag. **1**, 518 (1956).
[82]Other processes may contribute and a model, generalizing the five-frequency model of Lidiard and LeClaire, is needed for this situation.
[83]P. Erhart, in *Atomic Defects in Metals*, edited by H. Ullmaier, Landolt-Börnstein New Series III, Vol. 25 (Springer, Berlin, 1991), Chap. 2, p. 88.
[84]G. Henkelman, B. P. Uberuaga, and H. Jónsson, J. Chem. Phys. **113**, 9901 (2000).
[85]R. P. Smith, AIME Conf. Proc. **230**, 476 (1964).
[86]J. Ågren, Scr. Metall. **20**, 1507 (1986).
[87]A. D. LeClaire, in *Diffusion in Solid Metals and Alloys*, edited by H. Mehrer, The Landolt-Börnstein Database, Vol. 26 (Springer-Verlag, Berlin, 1990), p. 471–503.
[88]P. Thibaux, A. Métenier, and C. Xhoffer, Metall. Mater. Trans. A **38**, 1169 (2007).
[89]R. Lappalainen and A. Anttila, Appl. Phys. A **42**, 263 (1987).
[90]G. J. Thomas and R. Bastasz, J. Appl. Phys. **52**, 6426 (1981).
[91]H. K. D. H. Bhadeshia, J. Mater. Sci. **39**, 3949 (2004).
[92]K. Oda, H. Fujimura, and H. Ino, J. Phys.: Condens. Matter **6**, 679 (1994).
[93]H. Numakura, K. Kashiwazaki, H. Yokoyama, and M. Koiwa, J. Alloys Comp. **310**, 344 (2000).
[94]These results agree to within errors with our previous work[54] at a lower plane-wave cutoff energy and we direct the reader there for further discussion.
[95]T. Sourmail, Mater. Sci. Tech. **17**, 1 (2001).
[96]E. H. Megchiche, S. Pérusin, J.-C. Barthelat, and C. Mijoule, Phys. Rev. B **74**, 064111 (2006).
[97]E. H. Megchiche, C. Mijoule, and M. Amarouche, J. Phys.: Condens. Matter **22**, 485502 (2010).
[98]K. Tapasa, A. V. Barashev, D. J. Bacon, and Yu. N. Osetsky, Acta Mater. **55**, 1 (2007).
[99]G. J. Thomas, W. A. Swansiger, and M. I. Baskes, J. Appl. Phys. **50**, 6942 (1979).
[100]R. J. K. Nicholson and J. M. Walls, J. Nucl. Mater. **76-77**, 251 (1978).
[101]N. Yoshida, E. Kuramoto, and K. Kitakijima, J. Nucl. Mater. **103**, 373 (1981).
[102]E. C. Bain, AIME Conf. Proc. **70**, 25 (1924).